



Project of Strategic Interest NEXTDATA

WP1.2

(Coordinator: Marco Doveri, IGG-CNR)

D1.2B – Groundwater models for the selected Apennines and Alpine aquifer systems and integration of the D1.2A in terms of geological, hydrogeological and geochemical data concerning the Alpine aquifer

Authors: Marco Doveri, Matia Menichini, Brunella Raco, Giulio Masetti, Andrea Irace, Matteo Lelli, Barbara Nisi

IGG-CNR

This deliverable provides the numerical models of groundwater quantity elaborated for the three main aquifer systems involved in the project and located in central and northern Apennines and western Alps. It also integrates the first deliverable (D 1.2A) in terms of geological, hydrogeological and geochemical data and groundwater quantity and quality trends regarding the Alpine foothill aquifer.

Table of contents

1. INTRODUCTION	pag. 2
2. THE FOOTHILL AQUIFER SYSTEM OF THE PIEDMONT ALPINE ZONE	3
2.1. Geological, hydrogeological and geochemical setting.....	3
2.2. Synthesis of data and information into the aquifer conceptual model	14
2.3. Data of monitoring and trends	15
3. PHYSICALLY-BASED GROUNDWATER FLOW MODEL OF THE FOOTHILL ALPINE AQUIFER SYSTEM	24
3.1. Model implementation	24
3.2. Model calibration and results	31
3.3. Forecast simulation	35
4. EMPIRICAL GROUNDWATER QUANTITY MODELS OF THE APPENNINES AQUIFER SYSTEMS	36
4.1. Flowrate model of the Galleria Nuova spring – Mt. Amiata aquifer	37
4.2. Flowrate model of the Cartaro spring – Apuan Alps aquifer	43
5. CONCLUSIONS	48
REFERENCES	

1. INTRODUCTION

The Task 1 of the WP1.2 focus on groundwater, which represents, globally, the main resource in term of water supply (Martínez et al., 2008; Zhu and Balke, 2008; Hiscock, 2011; Baoxiang and Fanhai, 2011; Doveri et al., 2016). Particularly the Task focus on groundwater systems in mountain area, by dealing with quantity and quality issues of three main aquifers extended in Apennines and Alpine areas (Fig. 1.1). The conceptual model of aquifers is accounted by comparing physical and chemical features and an analyses of trends on groundwater quantity and quality is performed. Furthermore, numerical models are developed throughout either empirical or physically-based approach, accordingly the hydrodynamic conditions of aquifers and the availability of data and information. This overall approach can be considered a reference strategy for investigating mountain aquifers.

Within the first deliverable (D 1.2A) we mainly referred to the two systems in Central and Northern Apennines (Mt. Amiata and Apuan Alps systems), by providing their conceptual models and an analysis of the quantity and quality trends concerning their groundwater resources.

In this second deliverable we firstly provide a description and a trends analysis of the foothill system in the Alpine area, and then we focus on the numerical models elaborated for the three aquifer systems involved in the project. As already specified for the first deliverable, the data and information derive from studies and researches chiefly performed in close cooperation with water management companies and authorities, as well as from monitoring activities institutionally performed by regional governments and environmental agencies. For the foothill Alpine system, on which the present report mainly focuses, the study was performed in close cooperation with SMAT (Società Metropolitana Acque Torino), which also co-founded some activities.

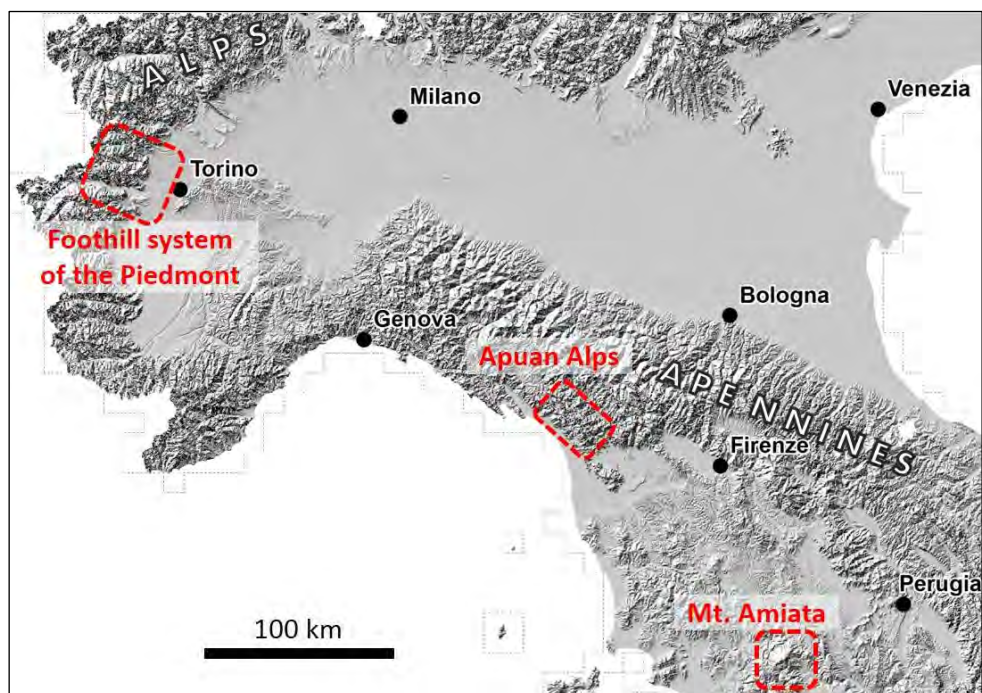


Fig. 1.1 – Apennine and Alps zones in which aquifer systems examined in the project extend.

2. THE FOOTHILL AQUIFER SYSTEM OF THE PIEDMONT ALPINE ZONE

2.1. Geological, hydrogeological and geochemical setting

The foothill aquifer system of the Piedmont Alpine Zone is here considered by focusing on the Torino area, which consists of a foothill plain developed in the western Piedmont region between the Western Alps and the Torino Hill (Piana et al. 2017; Fig. 2.1). This area is of special interest, since it represents the hydrogeological “transition zone” between the Western Po Plain and the southern Piedmont Plain aquifer systems (Irace et al. 2009, 2010). From a morphological point of view, the Torino plain gently slopes towards the East, from the Rivoli-Avigliana end-moraine system up to the Po River, on the edge of the Torino Hill.

This foothill plain is mainly made up of quaternary fluvial deposits of the Po River tributaries, which constitute a widespread blanket, overlaying the Pliocene succession.

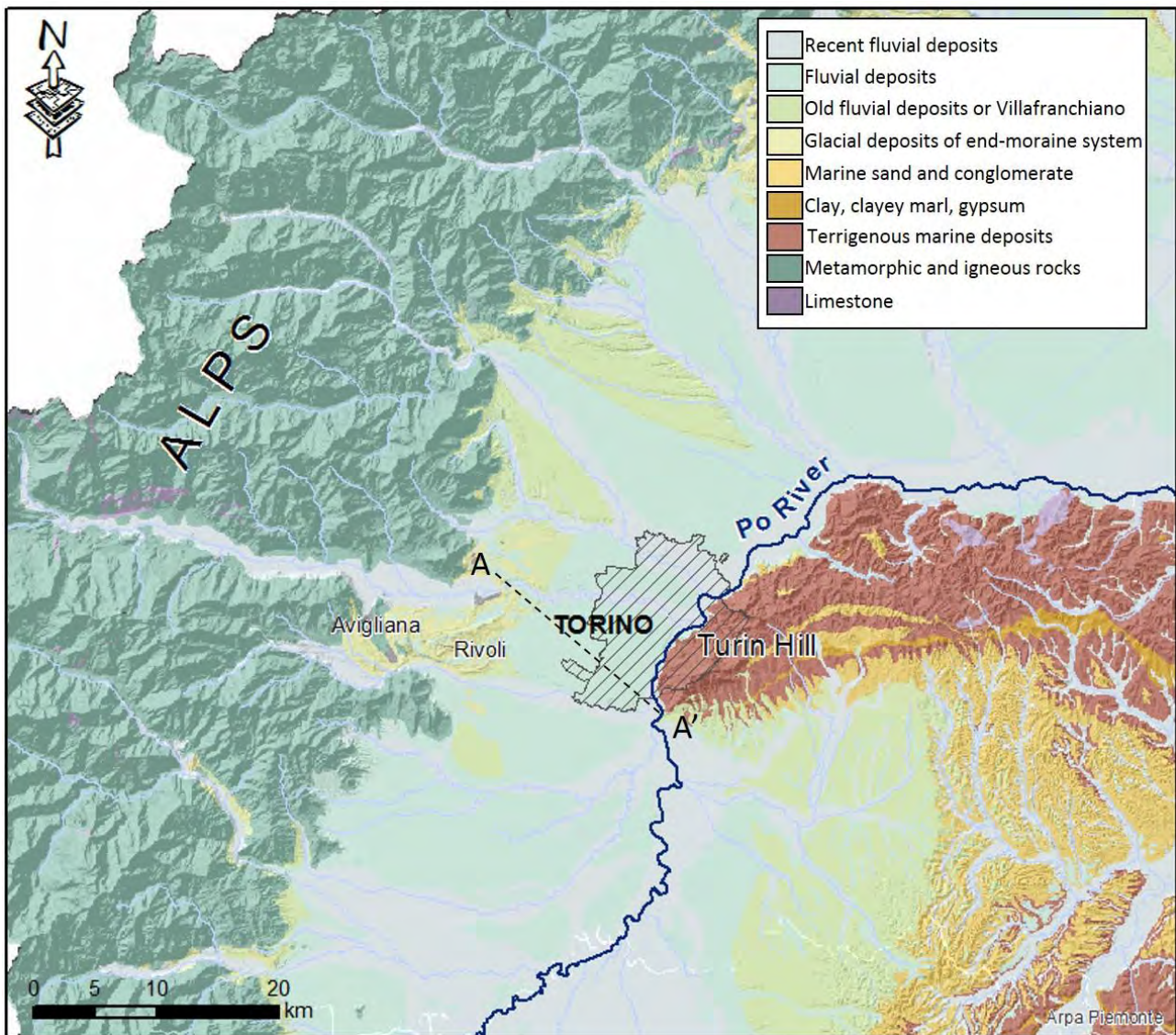


Fig. 2.1 - Simplified geological map of the western Piedmont region (modified from www.webgis.arpa.piemonte.it)

In this area, five main geological units are distinguishable and affect the general hydrogeological frame (Figs. 2.1- 2.2):

1. Metamorphic Crystalline rocks (mainly gneiss, micaschists, quartzites, ophiolitic units) in the inner edge of the Alpine chain. The fracture systems of these lithologies results in a reduced groundwater circulation, in agreement with the high runoff coefficient accountable for the Alpine basins of this area (http://www.arpa.piemonte.gov.it/rischinaturali/accesso-ai-dati/annali_meteoidrologici/annali-meteo-idro/banca-dati-idrologica.html);
2. Marine succession (Eocene-Miocene age) outcropping in the Turin Hill. Clays, marls, silts, clayey limestone, conglomerates, sandstone, and gypsum mainly compose this unit. These lithologies have low permeability and only a limited groundwater circulation along fault zones that feeds springs with very low flowrate.
3. The Pliocene complexes involving both Continental Deposits (Villafranchiano *Auct*), which are represented by a succession of sandy gravel and silty clay, and Marine Deposits (AST and FAA), which consist of sandy (Sabbie di Asti-AST) and silty clayey facies (Argille Azzurre-FAA). The sandy gravels of Villafranchiano and, locally, the Sabbie di Asti host important groundwater resources.
4. Glacial deposits of Rivoli end-moraine system. These deposits are extremely heterogeneous, with lithologies from blocks to clays and, as a whole, they are characterized by a very low permeability.
5. Alluvial, fluvioglacial and megafan deposits (Pleistocene-Holocene) consist of gravel and sandy gravel with high permeability. These deposits host an important phreatic aquifer widely studied and exploited.

The present project activity focuses on the aquifer system that encompasses the *Pliocene* and *Pleistocene-Holocene sequences*, which represent two sub-systems respectively hosting a confined to semiconfined multilayer aquifer system and a regional phreatic aquifer.

The Pliocene sub-system

Below the quaternary cover, the Pliocene succession defines a km-scale NNE-SSW trending footwall syncline overthrust by the Torino Hill anticline, along the “Padane Front” NW-verging thrust system (PTF). The Pliocene sedimentary stack is several thousand meter thick (about 800m) in the axial portion of the Torino plain and progressively thins towards the western and eastern margins.

To the West, Pliocene deposits directly cover the Alpine basement, whereas to the East, they unconformably rest onto the Miocene successions of the north-western limb of the Torino Hill anticline (Fig. 2.2).

The Pliocene transgressive-regressive sequence constitutes a large scale prograding prism generated by the southeastward regression of deep- to shallow-marine depositional systems that from base to top became progressively transitional and finally continental. In detail, the Pliocene succession is represented by: the “**Argille Azzurre**” basin to outer shelf deposits (FAA), the “**Sabbie di Asti**” inner shelf to tide-dominated nearshore deposits (AST), and the continental deposits, up to date generically ascribed to the “**Villafranchiano Auct.**” informal

unit (Martinetto et al., 2007). This term is still in use in the Piedmont region solely for historical reasons and designates the non-marine deposits, which conformably overlay the Pliocene marine successions. These successions were referred to the “Unità di La Cassa” (LSS) by recent geological mapping (Balestro et al., 2009).

Due to the progradational stratigraphic architecture, the Pliocene succession shows interfingering of continental and marine deposits, spanning from Zanclean to Piacenzian.

All along the eastern border of the area, Miocene and Pliocene strata are uplifted and displaced by the PTF fault system (Fig. 4.2). In this sector, the “Unità di La Cassa” continental deposits are lacking, and the FAA and AST form a nearly continuous N-S directed morpho-structural “plateau”, unconformably followed by the fluvial and fluvio-glacial Pleistocene-Holocene sequence.

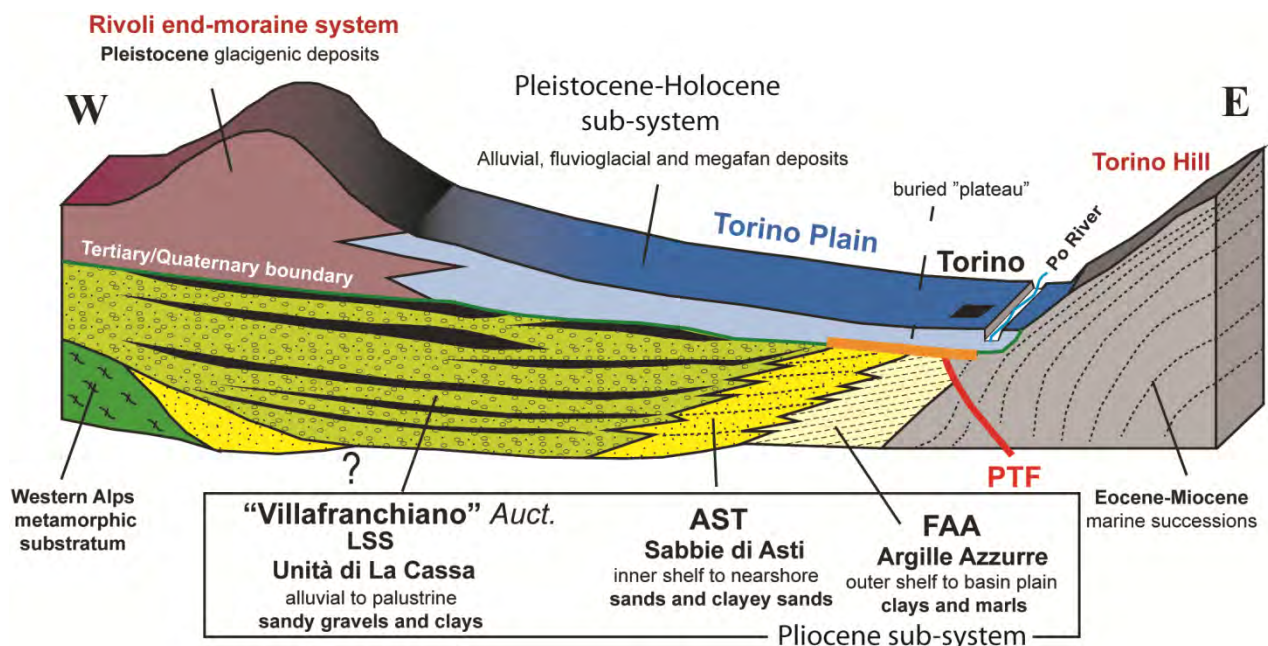


Fig. 2.2 - Simplified geological 3D-scheme (modified from De Luca and Ossella, 2014)

The FAA mainly consists of clays and marls with subordinated laterally continuous arenite layers (lower part), thus corresponding to regional-scale aquitard/aquiclude.

The AST mainly consists of fine- to coarse-grained sand to arenite amalgamated sedimentary bodies. The permeability of sandy layers is somewhat variable and generally ranges from relatively high to intermediate values. However, the abundant inter-granular clayey matrix, often characterizing the sands, reduces the potential of water exploitation from this hydrogeological unit.

The “Unità di La Cassa” (LSS; “Villafranchiano Auct.”) reaches maximum thickness of about 200 m below the axial part of the Torino plain. From depocentral areas, it markedly tapers toward present day western and eastern margins. The LSS thins out towards the East, on the buried “plateau” of tertiary marine sediment, bordering the Torino Hill (Fig. 2.2).

The LSS marks the onset of continental sedimentation in the area and it testifies the progradation from the western Alps of alluvial plain and palustrine/lacustrine depositional systems, southeastward grading into coeval shelfal systems of the AST. The LSS consist of coarse-grained sands and gravels, alternating to peat-rich clayey and silty deposits.

This alternation of deposits with high permeability and others with low permeability result in a mainly confined to semiconfined multilayer aquifer system, which locally can have an unconfined character where the permeable layers are directly in contact with the overlying Pleistocene-Holocene Unit. As a whole, the lateral persistence and thickness of interlayered fine grained bodies increases moving away from the source areas, so that the semi-confined (even locally unconfined) aquifer system becomes confined eastward (Fig. 2.3). This evolution of the hydrogeological condition moving towards the Po River is also retained as a possible favourable effect in the origin of the “fontanili” (typical lowland springs occurring in Northern Italy along the transition zone from the higher to lower plain) that are widespread in the Turin Po Plain (De Luca et al., 2014). Values of average hydraulic conductivity of this system range from $4 \cdot 10^{-5}$ to $4 \cdot 10^{-4}$ m/s (De Luca and Osella, 2014). This aquifer system is the most exploited in the area, also for its particular natural protection from pollution. In fact, the different confined aquifer layers are generally separated each other and from the overlying phreatic aquifer hosted in the Pleistocene-Holocene fluvio-fluvioglacial deposits. Nevertheless, in upper land of the foothill area the LSS deposit together with the overlying Pleistocene-Holocene fluvio-fluvioglacial deposits constitute a unique and powerful phreatic aquifer (Fig. 2.3). The perialpine area is therefore to be considered the recharge area of the Pliocene multilayer aquifer system and to be protected from pollution.

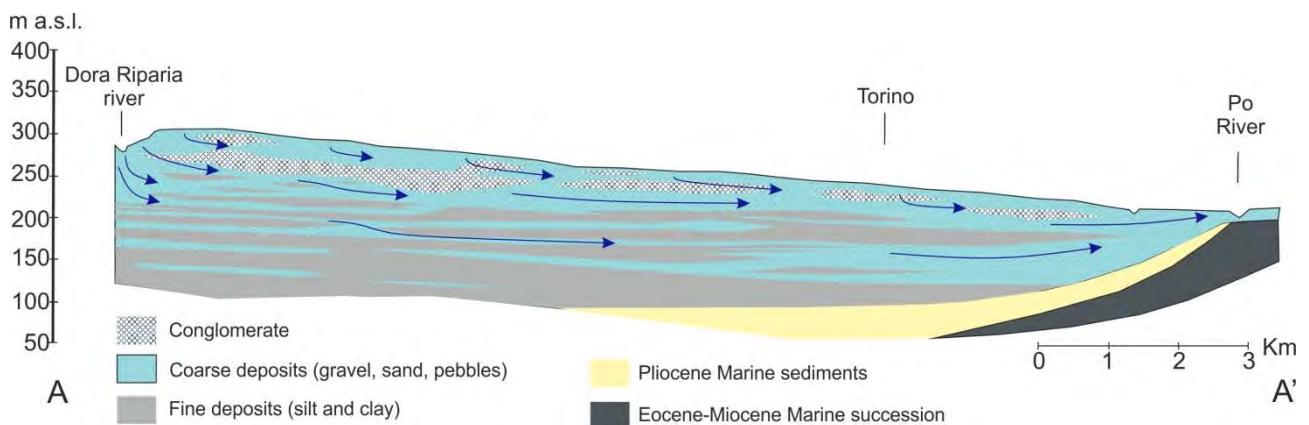


Fig. 2.3 - Simplified hydrogeological section (modified from Canavese et al., 2004). The section trace is shown in figure 2.1.

The Pleistocene-Holocene sub-system

The Pleistocene-Holocene deposits consists of gravel and sandy gravel with pebbles of fluvial and fluvioglacial origin, with increasing granulometry to the west. These deposits mostly overlay the LSS. Only along a narrow strip parallel to Turin Hill they overlay the marine tertiary

substrate (Figs. 2.2 e 2.3). The thickness of these deposits range from a maximum of 80 m in the west area to about 30 m to the east, near the Po River.

The deposits host a phreatic aquifer, widely studied (Lucchesi, 2001; Capilongo et al., 2003; Canavese et al., 2004; Lo Russo and Taddia, 2009; De Luca and Ossella, 2014; De Luca et al., 2014) and monitored (§ 2.3). Also this aquifer is deeply exploited for drinking water, agricultural and industrial purposes, even if their vulnerability is higher than the Pliocene sub-system aquifers (AST and LSS).

The water table depth ranges from 50 meters, in the perialpine sector, to about 5 m in the sector closest to the Turin Hill. The average value of hydraulic conductivity, obtained by aquifer tests, varies from $5 \cdot 10^{-4}$ m/s, to $5 \cdot 10^{-3}$ m/s (De Luca and Osella, 2014). This aquifer is mainly fed by direct rainfall and river at the outlet of the alpine valleys in the plain. The water table of this shallow aquifer is directly connected to the superficial hydrographic network.

The piezometric map in the figure 2.4 was elaborated basing on measurements performed in shallow wells (data from www.webgis.arpa.piemonte.it). It therefore refers to the shallow and phreatic aquifer (*Pleistocene-Holocene sub-system*). Nevertheless, over wide sub-zones it can be considered as representative of the ensemble “shallow aquifer-uppermost layers of the deeper system”, given the above discussed possible connection between the two sub-systems. The map shows a main groundwater flow from northwest to southeast in the northern part of the plain, and from west to east in the southern sector. In particular, in the area of interest (Torino plain) the groundwater flow is generally towards the Po River, which mainly seems to act as drainage of the aquifer system. Also some main tributaries act as drainage of the aquifer (i.e. Stura di Lanzo, Orco, Malone, and Chisola river). As regards the Dora Riparia River, in the inner zone it flows at altitudes 10-15 m higher respect to piezometric levels, thus excluding the continuity between stream and groundwater flow, as already discussed by De Luca et al., 2014. Nevertheless, the shape of the piezometric curves suggests a possible river seepage towards groundwater, although the stream remains disconnected from the water table. This relationship “stream water-groundwater” is in agreement with the high permeability of sediments, which promote the seepage, and the significant groundwater withdrawal, which causes a significant piezometric drawdown in this sector. Moving toward Torino Hill, the difference in elevation between the Dora Riparia River and the water table is progressively reduced, and a few kilometers upstream the confluence with the Po River the Dora Riparia River is connected with the water table and continue to feed the aquifer.

The hydraulic gradient of the piezometric surface are between 1%, in the higher sector, close to the Alps, and 0.1 % in the distal sector, nearby to the Po River.

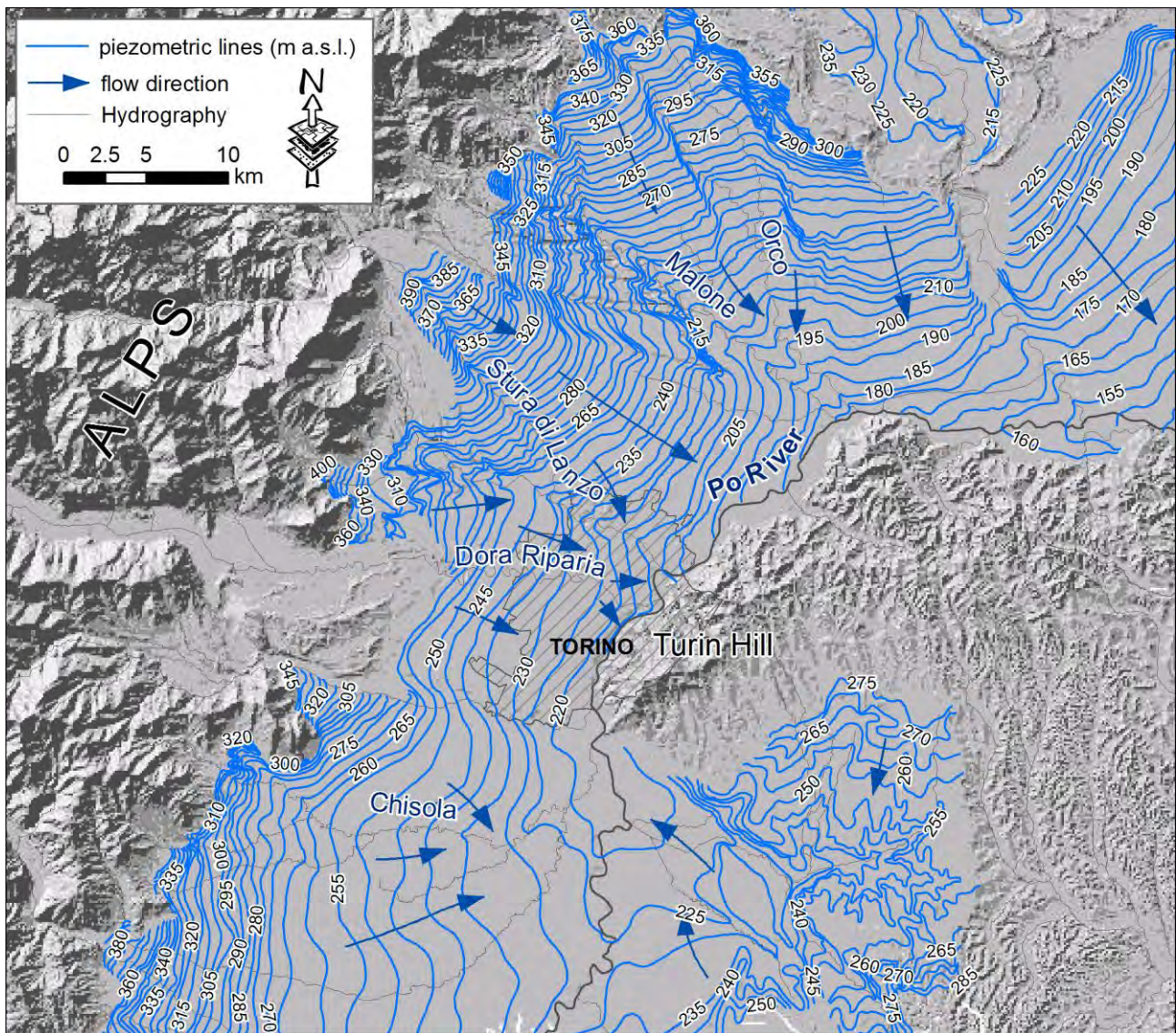


Fig. 2.4 - Piezometric map of the Torino Po plain, elaborated upon values measured in shallow wells (June-July 2002, data from www.webgis.arpa.piemonte.it).

From a geochemical point of view, this report takes into account data of 2127 chemical analyses coming from the groundwater-monitoring network of the Environmental Protection Agency of Piedmont Region (ARPAP). According to the subdivision made by ARPAP, 1191 analyses are related to shallow groundwater, whereas 936 analyses refer to “deep groundwater”. In first instance, we associated the first 1191 analyses to the phreatic aquifer (PA, hereafter) and the remaining 936 to the deeper aquifer system characterized by confined to semi-confined conditions (CA, hereafter).

As a whole, these data refer to a total of 138 wells (Fig. 2.5), which are monitored since 2002 by means of two annual surveys; 59 wells develop up to the confined/semi-confined aquifer system, and 79 wells are in the phreatic one. It has to be underlined that in many cases the deeper wells can drain all permeable layers they cross, thus tapping water in both PA and CA aquifers. Therefore, the differentiation above discussed in terms of chemical analyses representativeness not always results rigorous.

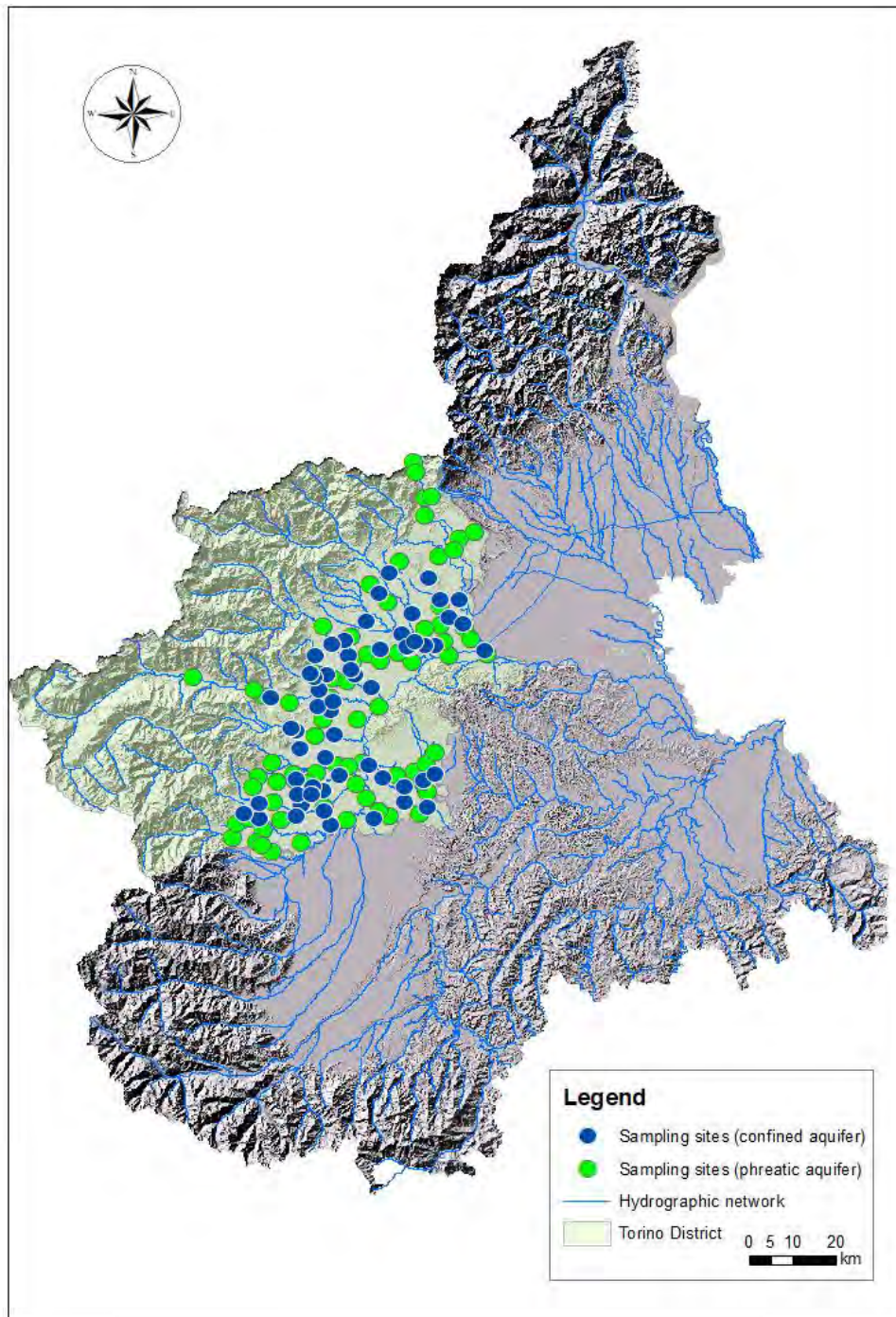


Fig. 4.5 - Location of ARPAP wells monitoring network.

The analytical quality of available data was first checked taking into account the “principle of electroneutrality” of the aqueous solution:

$$CB\% = \frac{|\sum cations - \sum anions|}{\sum cations + \sum anions} \cdot 100$$

The analytical data with charge balances exceeding the 10% threshold have been excluded in the data processing. 50 analysis related to PA and 65 analysis linked to the CA did not satisfy this quality criterion.

A classical approach, based on triangular diagrams, was used in order to investigate the chemical facies of groundwater. Figures 2.6-2.7 show the triangular plots $\text{HCO}_3\text{-Cl-SO}_4$ and Ca-(Na+K)-Mg for PA and CA, respectively.

Triangular diagrams that refer to PA show the dominance of samples with bicarbonate-alkaline-earthly composition, respect to a few exceptions. These latter consist of waters of the sulfate-calcium type that refer to samples from FROSSASCO station and some samples from ORBASSANO and COLLEGNO stations. Another exception is represented by samples taken at POIRINO station that show a sodium-chloride composition. Furthermore, the diagrams highlight the presence of a few bicarbonate-magnesium waters (GIVOLETTO, FAVRIA, AIRASCA and MONTANARO stations).

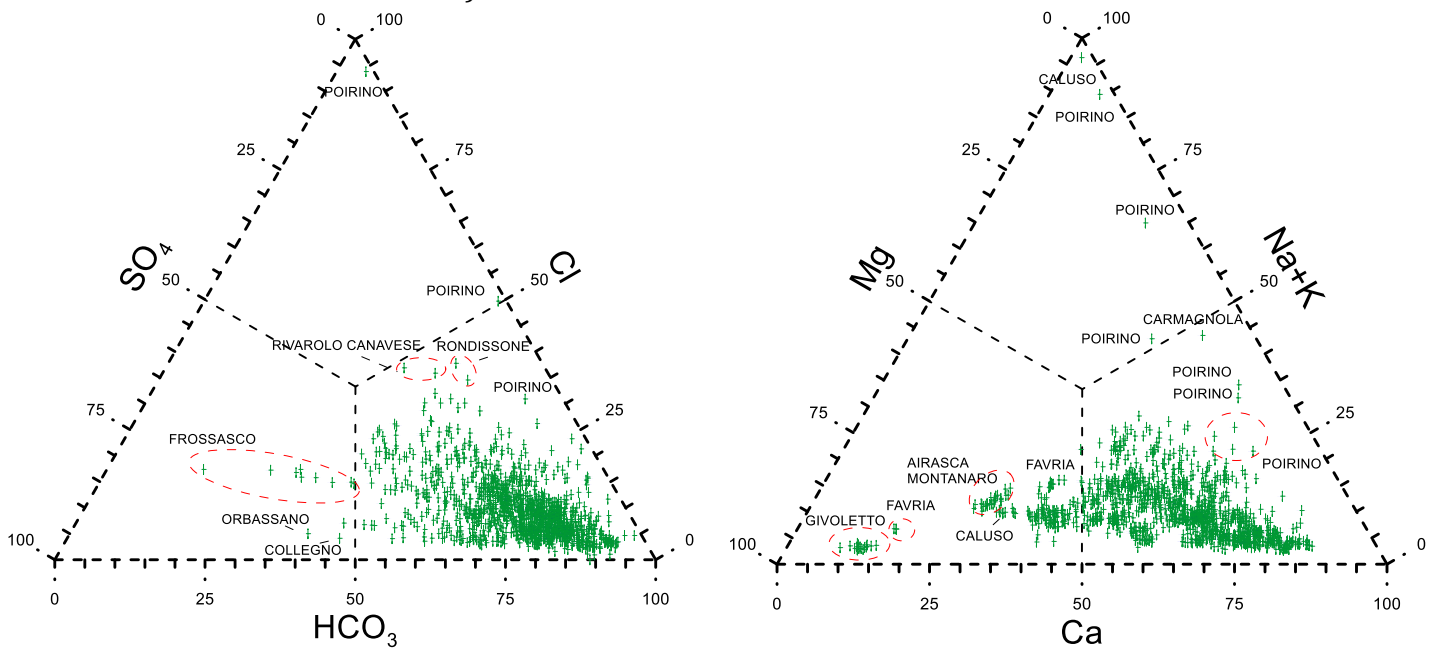


Fig. 2.6 - Triangular plots of anions and cations for PA waters

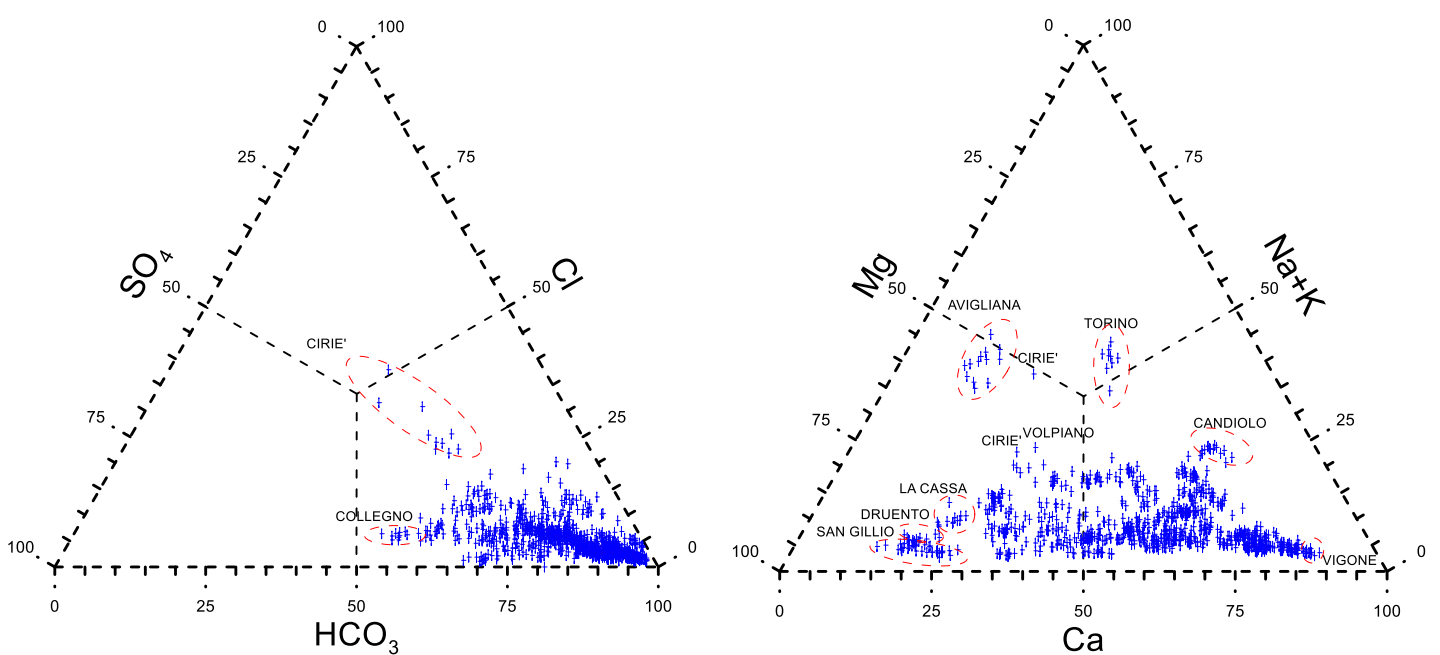


Fig. 2.7 - Triangular plots of anions and cations for CA waters

All the samples of the CA wells have a bicarbonate-alkaline-earthly facies (Fig. 2.7). Most water is of the bicarbonate-calcium type, whereas a few samples show a bicarbonate-magnesium composition (SAN GILLO, DRUENTO and LA CASSA stations) or a higher alkaline content (AVIGLIANA and TORINO stations). In a few cases it is showed a relative enrichment in sulfate-calcium content (COLLEGNO station), as well as a relative enrichment in chloride (CIRIE' station).

In short, the classification diagrams indicate the presence of:

- (i) Waters with bicarbonate-alkaline-earthly facies: these represent the majority of the samples belonging to both the CA and PA.
- (ii) Intermediate waters: in this case none of the three anions exceed the 50% of total normalized anion content. Nevertheless, the main part of these samples show a prevalence of HCO_3 . Some exceptions are present: for the PA, SO_4 is the main anion in all FROSSASCO samples and in one sample of ORBASSANO station, whereas chloride is present as major anion just in one sample of the POIRINO station. For what concern the CA, SO_4 is the main anion of some samples of CIRIE' station and of one sample of COLLEGNO monitoring point, whereas Cl is the main anion just for one sample of SAN BENIGNO CANAVESE station.
- (iii) Waters with Cl-alkaline facies: the only water that show this facies is a POIRINO sample (PA). This sample is not reported in the diagram of figure because it reaches a total salinity of 233 meq/L. This facies is not present in the CA.
- (iv) Waters with sulfate facies: only a few water samples of the PA belong to this chemical type, and in particular one sample collected at the ORBASSANO station, one sample collected at the COLLEGNO station and three samples from FROSSASCO monitoring well. For these waters, the dominant cationic specie is Ca.

The discussed diagrams do not consider the total ion salinity (SIT) of waters. This important information can be retrieved from the diagram of Figure 2.8, where the sum $\text{Cl} + \text{SO}_4 + \text{Na} + \text{K}$ is compared to the sum $\text{HCO}_3 + \text{Ca} + \text{Mg}$.

The maximum salinities, greater than 20 meq/L, are reached by the samples linked to phreatic aquifer, in particular, by the POIRINO monitoring station and by one sample related to the ROSTA station. In general, the total salinity is low, and water related to CA have a total salinity lower than PA. These low values are typical of meteoric water with very low grade of interaction with hosting rocks.

The spatial distribution of hydrochemical facies of PA is shown in Fig. 2.9. The map shows the presence of two areas characterized by a higher density of intermediate facies, one located on the orographic right of Chisola stream (PINEROLO, FROSSASCO, PISCINA, AIRASCA, CUMIANA) and one situated in proximity of the south-east border of Torino province (CARMAGNOLA, POIRINO, RIVA PRESSO CHIERI). The other monitoring wells showing change in hydrochemical facies are COLLEGNO (about 50m far from Doria Riparia river), RIVAROLO CANAVESE e FAVRIA (located between Orco and Malore rivers) and RONDISSONE (located 1 km far from right side of Dora Baltea river). The occurrence of these variations in hydrochemical facies may indicate the presence of interaction processes among PA with the

hydrographic network, in agreement with the piezometric surface. Moreover, changes in hydrochemical facies could be due to local input of meteoric water or anthropic input (sewers, fertilizers, ...) as suggest by samples of POIRINO station located near the cemetery, or samples coming from urban areas like those of the FROSSASCO station.

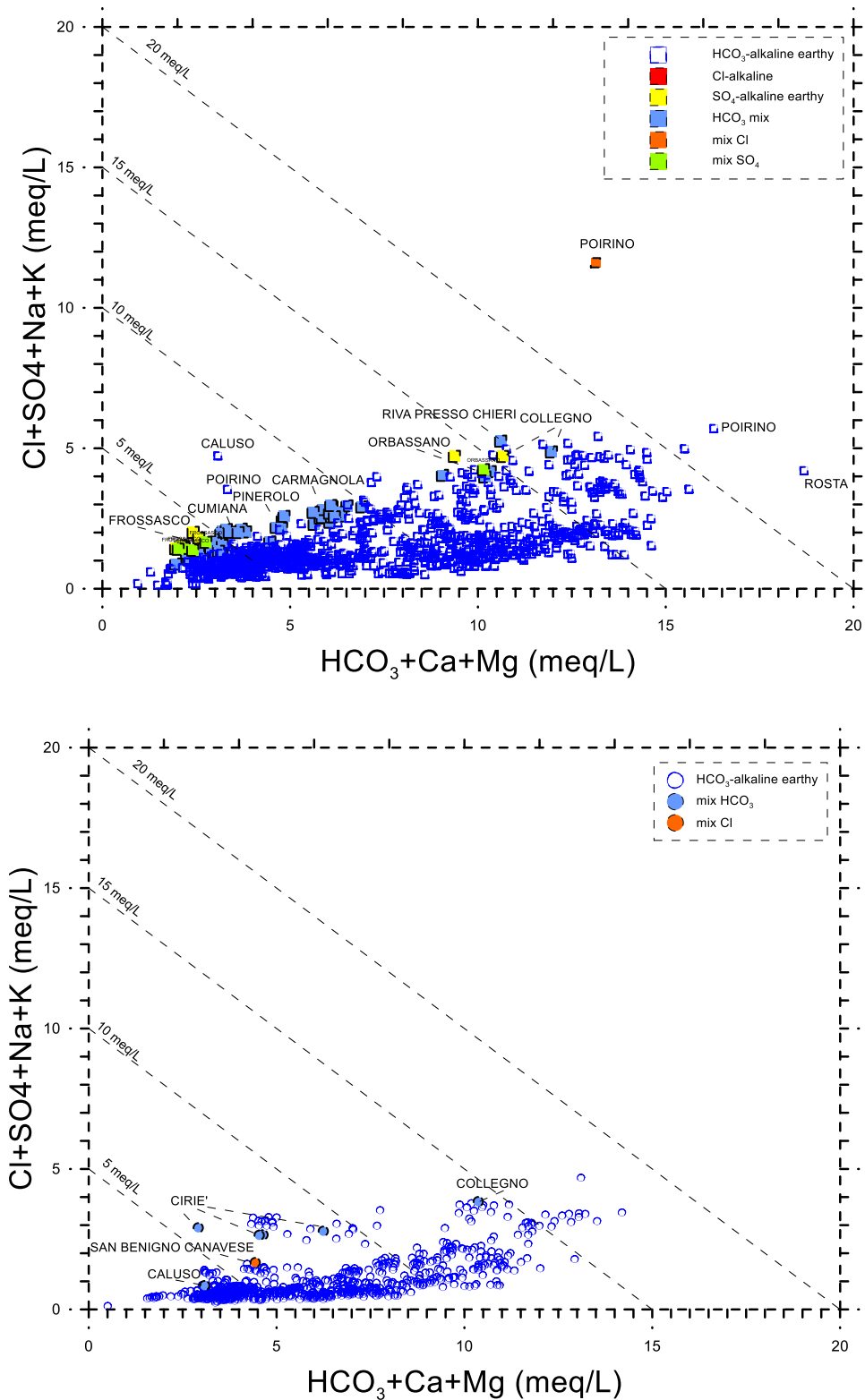


Fig. 2.8 - Total salinity diagrams referred to the phreatic aquifer (above) and confined/semi confined aquifer (below).

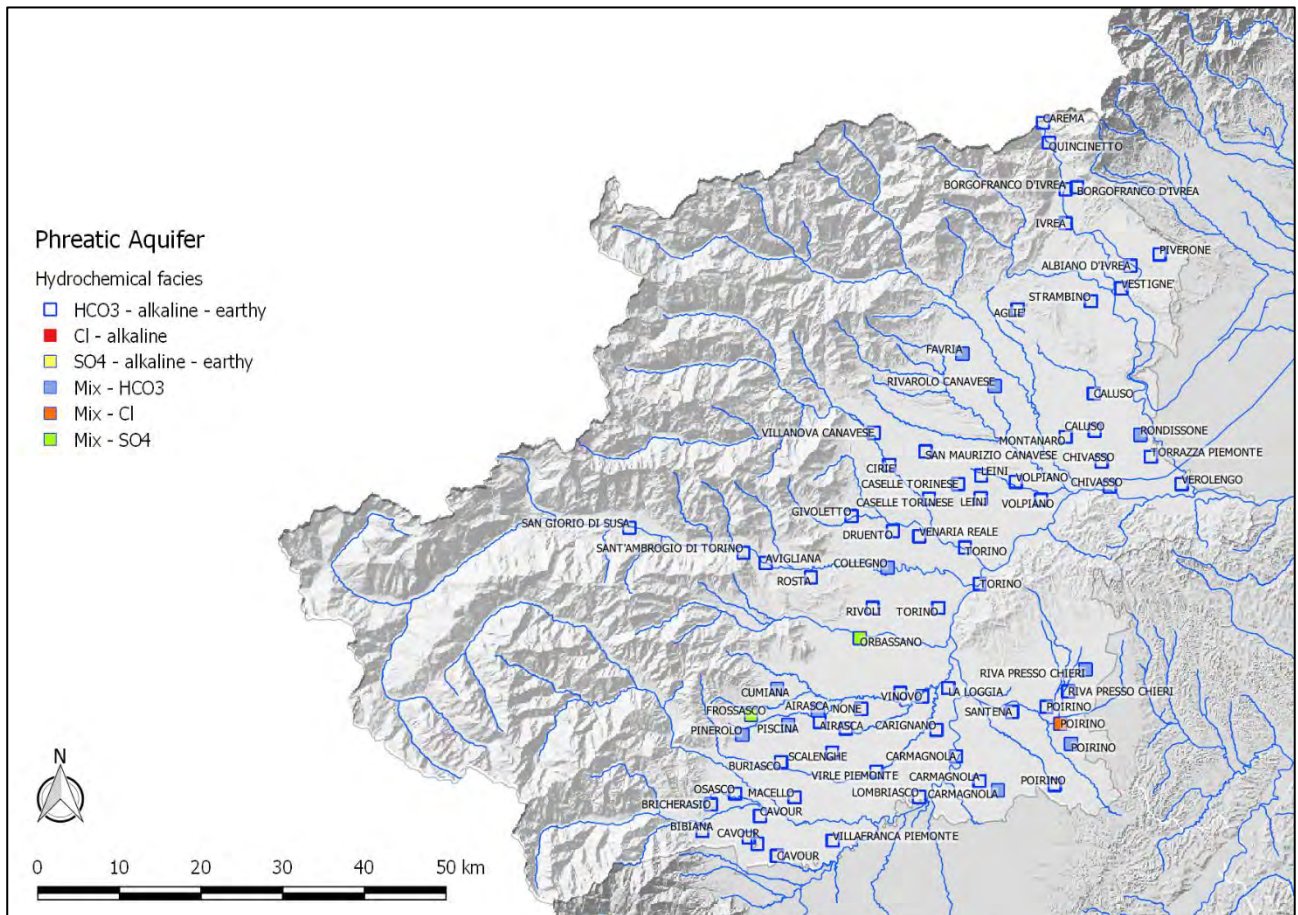


Fig. 2.9 - Spatial distribution of hydrochemical facies of the PA.

The spatial distribution of hydrochemical facies of the CA is shown in Figure 2.10. The map shows that almost all stations are steadily characterized by HCO₃⁻ alkaline earthy facies. Only four stations show HCO₃⁻ intermediate waters, and in one case is present a Cl intermediate water. The observed variability of these four monitoring wells could be due to interaction with phreatic aquifer as suggested by the Cl content (>20mg/L) and with hydrographic network. This last hypothesis comes from the proximity of these monitoring points to local rivers.

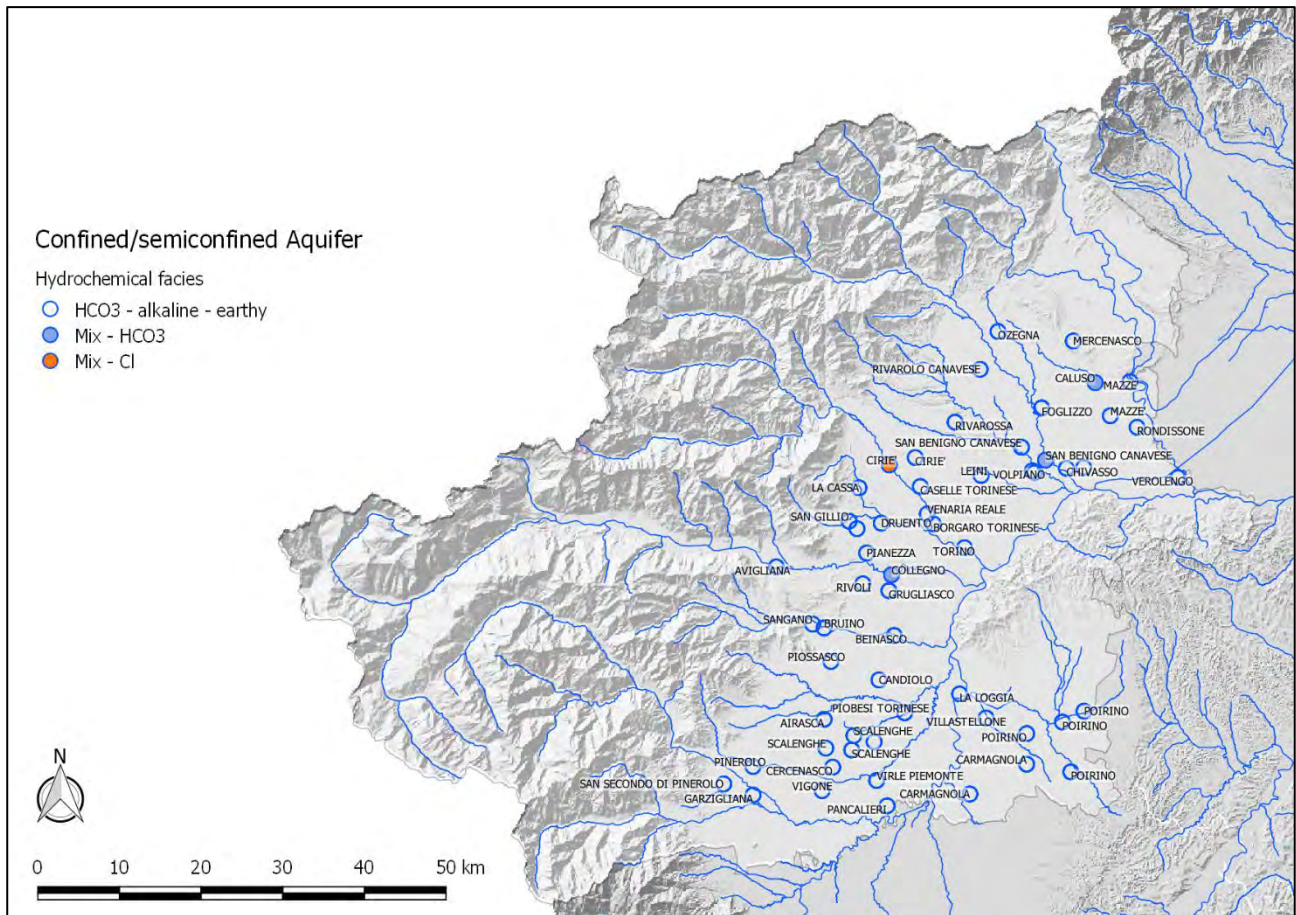


Fig. 2.10 - Spatial distribution of hydrochemical facies of the CA.

2.2. Synthesis of data and information into the aquifer conceptual model

The foothill aquifer system that develops under the Torino Plain is considered the most important reservoir in the Torino Province (Bove et al. 2005), given its extension, the texture of its sediments and the large natural recharge occurring in this area. The main features of this system can be summarized as follows:

- it consists of a multilayer aquifer systems that has a phreatic aquifer overlying a succession of impermeable and permeable layers, in which groundwater flow generally occurs in confined to semi-confined conditions;
- the phreatic aquifer has thicknesses between 30 and 80 m and it is hosted in gravel, sandy gravel and pebbles of fluvial and fluvio-glacial origin (Pleistocene-Holocene deposits). The hydraulic conductivity ranges from $5 \cdot 10^{-4}$ m/s to $5 \cdot 10^{-3}$ m/s;
- the confined to semi-confined sub-system mainly develops within the Pliocene continental deposits, which consist of coarse-grained sands and gravels, alternating to peat-rich clayey and silty deposits. The average hydraulic conductivity of this system ranges from $4 \cdot 10^{-5}$ to $4 \cdot 10^{-4}$ m/s;
- the aquifer system is fed by infiltration of local rainfall, river seepage and transfers of groundwater that originate in upland zones (Fig. 2.11). The outputs of groundwater is for exploitation by wells and for drainage operated by rivers, in the lower part of the plain.

Generally, the groundwater flow of the phreatic aquifer is separated from that of the confined to semi-confined sub-system. Nevertheless, over wide zones the shallow aquifer and the uppermost permeable layers of the deeper system result in continuity (or separated by weak thicknesses of clayey deposits), thus making possible the mixing of groundwater between the two sub-systems. The main groundwater flow paths occur from northwest to southeast and from west to east;

- groundwater are mainly of the Ca(Mg)-HCO₃ type with a relatively low salinity for both unconfined and confined aquifers. Nevertheless, the phreatic aquifer hosts groundwater with a relatively higher salinity and, in some zones, characterized by increasing of Cl and SO₄ contents. Hence, a certain impact from anthropic activities seems to be possible. In this terms, the confined to semi-confined sub-system appears effectively more protected, even though the higher salinity and Cl contents observed in a few deeper wells suggest the possibility of connection with the shallower aquifer.

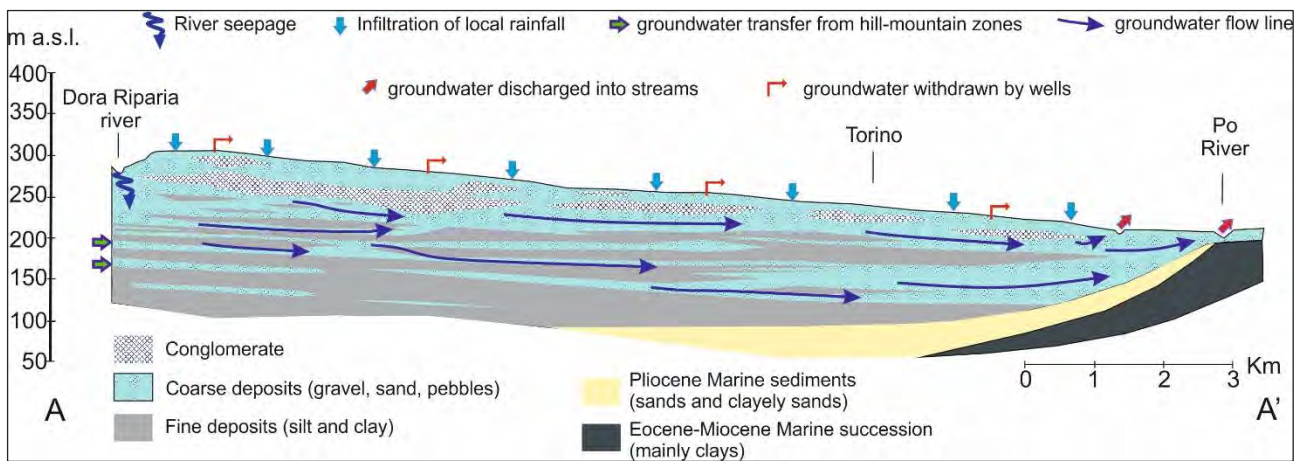


Fig. 2.11 – Schematic model of groundwater inputs and outputs.

2.3. Data of monitoring and trends

This section provides a presentation and a discussion of the monitoring data of piezometric levels and chemical compounds. The raw data are available at the following web pages:

1- GREASE: portal of Piedmont Region -

<http://www.regione.piemonte.it/monitgis/jsp/cartografia/mappa.do>;

2 - website of Metropolitan City of Torino-

<http://www.cittametropolitana.torino.it/cms/ambiente/risorse-idriche/progetti-ridriche/rete-monitoraggio/acque-sotterranee>

The Grease portal consists of a monitoring network with 33 wells/piezometers rather consistently distributed in the Torino Po plain (Fig. 2.12) and measuring the water level every 6/8 hours. In the table 2.1 are reported the code, the coordinates, the altitude, the depth and the measuring period for piezometric level.

In the website of the Metropolitan City of Torino the daily measurements of water level for 10 wells are available. These monitoring stations are mainly located on the southern edge of

Torino (Fig. 2.12). In the table 2.2 some technical characteristics are shown for this monitoring network (coordinates, depth, altitude, measuring period).

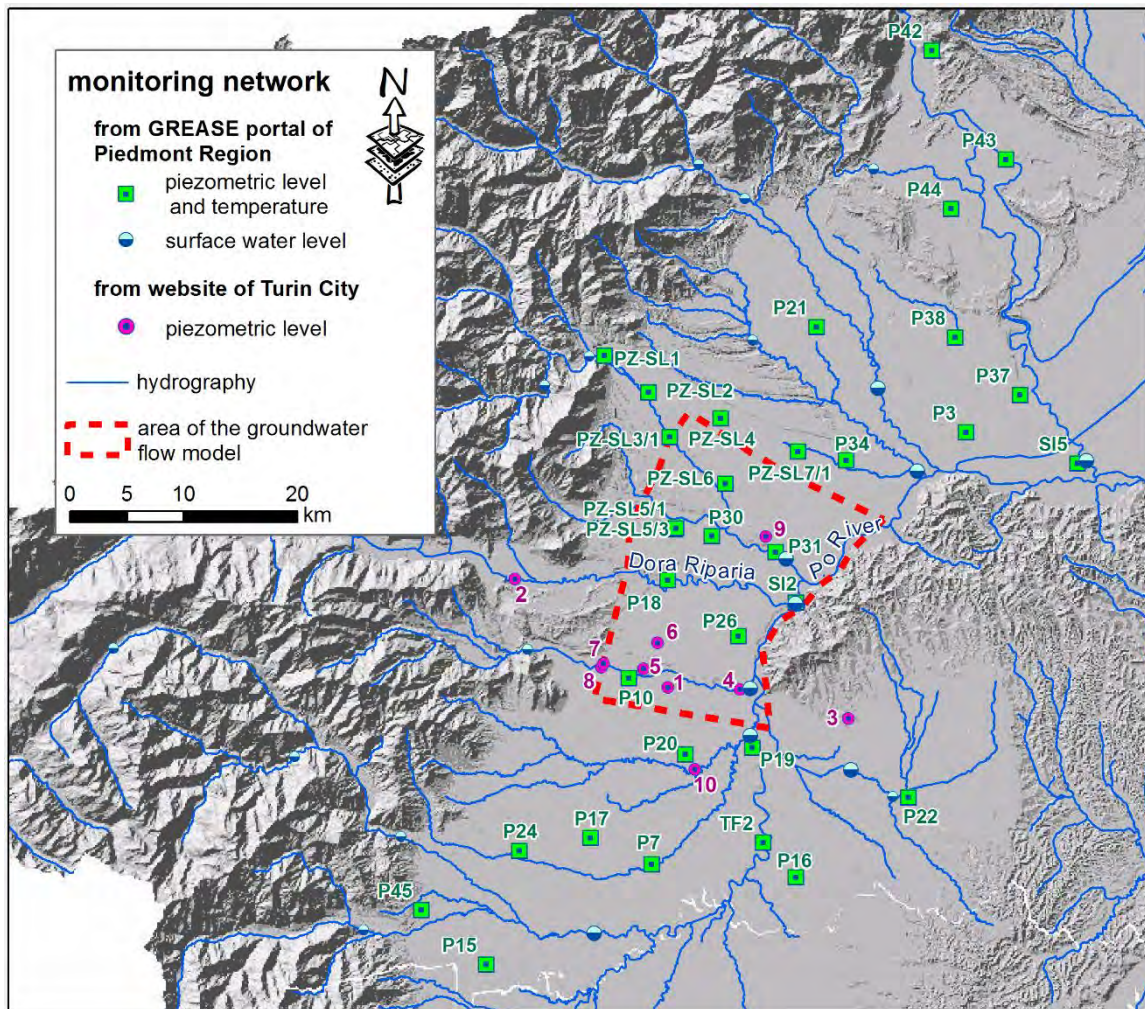


Fig. 2.12 – Monitoring network of piezometric level and surface water level in the Torino plain.

Piezometric data were compared with the rainfall (Fig. 2.13) that are representative of the area of interest and are derived from the “Optimal Interpolation” performed by ARPAP on weather stations data. A similar behavior of the piezometric levels is observed across the whole studied area. A sharp increase of levels occurred in the period 2008-2009 because of the rainier conditions. At the same time, over the 2009-2017 period most piezometers shows a significant trend of GW decreasing (confidence level of the trend is 95% to 99%) in response to the slight decreasing of rainfall. These patterns testify the high sensitivity of the aquifer system to the hydro-climatic conditions.

Code	X (UTM)	Y (UTM)	Altitude (m a.s.l.)	Depth	piezometric level monitoring period	
					from	to
P43	417575	5031188	229	24	16/02/2001	31/12/2016
P42	411034	5040779	254	25	16/02/2001	05/05/2016
P45	366209	4965240	384	42	23/02/2001	31/12/2016
P24	374793	4970404	301	35	15/04/2005	31/12/2016
P38	413095	5015532	259	53	20/06/2002	31/12/2016
P20	389400	4978896	237	20	18/08/2005	27/12/2016
P16	399090	4968086	238	25	11/01/2001	31/12/2016
TF2	396221	4971140	233	15	29/05/2002	31/12/2016
PZ-SL6	392908	5002669	279	20	24/03/2005	12/11/2016
P15	371891	4960419	299	30	15/04/2005	31/12/2016
P3	414045	5007210	196	30	15/03/2005	31/12/2016
PZ-SL3/1	388033	5006816	330	20	02/02/2006	31/12/2016
P18	387843	4994227	275	30	21/03/2005	31/12/2016
PZ-SL5/3	388492	4998701	274	20	25/03/2011	13/09/2016
PZ-SL5/1	388593	4998761	273	20	25/03/2005	18/03/2008
P19	395275	4979497	226	35	11/01/2001	31/12/2016
PZ-SL1	382287	5013929	441	15	24/03/2005	31/12/2016
PZ-SL7/1	399295	5005512	252	20	12/10/2005	31/08/2014
P10	384444	4985598	274	25	11/04/2005	31/12/2016
P22	408984	4975114	238	15	15/03/2001	17/11/2008
P21	400952	5016458	266	20	24/03/2005	31/12/2016
P37	418795	5010476	208	25	20/02/2001	31/12/2016
PZ-SL4	392480	5008458	319	20	10/03/2005	31/12/2016
P17	381057	4971571	258	25	11/01/2001	31/12/2016
P44	412735	5026842	232	25	16/02/2001	12/09/2016
SI2	399111	4992232	232	20	25/03/2005	13/05/2016
P31	397310	4996691	224	30	16/02/2001	13/12/2011
P26	394050	4989295	247	42	22/01/2001	31/12/2016
P30	391725	4998065	263	35	16/01/2001	31/12/2016
SI5	423848	5004454	177	20	15/03/2005	31/12/2016
PZ-SL2	386161	5010730	380	20	10/03/2005	31/12/2016
P7	386457	4969232	246	20	11/04/2005	31/12/2016
P34	403540	5004733	218	20	16/02/2001	23/10/2016

Tab. 2.1 – Code, coordinates, altitude, depth and measuring period for piezometric level of the monitoring network of the portal Grease (<http://www.regione.piemonte.it/monitgis/jsp/cartografia/mappa.do>)

Code	Name	X (UTM)	Y (UTM)	Altitude (m a.s.l.)	Depth	piezometric level monitoring period	
						from	to
1	Beinasco discarica	387872	4984753	250	15	27/09/2012	26/09/2016
2	Buttiglera Alta	374420	4994304	338	20	24/09/2009	09/11/2016
3	Cambiano consorzio	403730	4982031	262	55	16/12/2008	09/11/2016
4	Moncalieri Berval	394172	4984571	233	-	20/02/2014	26/09/2016
5	Orbassano discarica	385698	4986399	263	-	20/02/2014	08/11/2016
6	Orbassano Servizi	386917	4988695	283	51	14/03/2013	15/11/2016
7	Rivalta exchimica	382020	4986542	291	-	20/03/2014	26/09/2016
8	Rivalta Parco	382183	4986867	289	-	20/03/2014	26/09/2016
9	Torino Amiat	396455	4998050	226		21/06/2012	15/11/2016
10	Vinovo	390242	4977573	233	10	31/03/2009	09/11/2016

Tab. 2.2 – Code, name, coordinates, altitude, depth and measuring period for piezometric level of the monitoring network of the website of Turin city (<http://www.cittametropolitana.torino.it/cms/ambiente/risorse-idriche/progetti-ris-idriche/rete-monitoraggio/acque-sotterranee>)

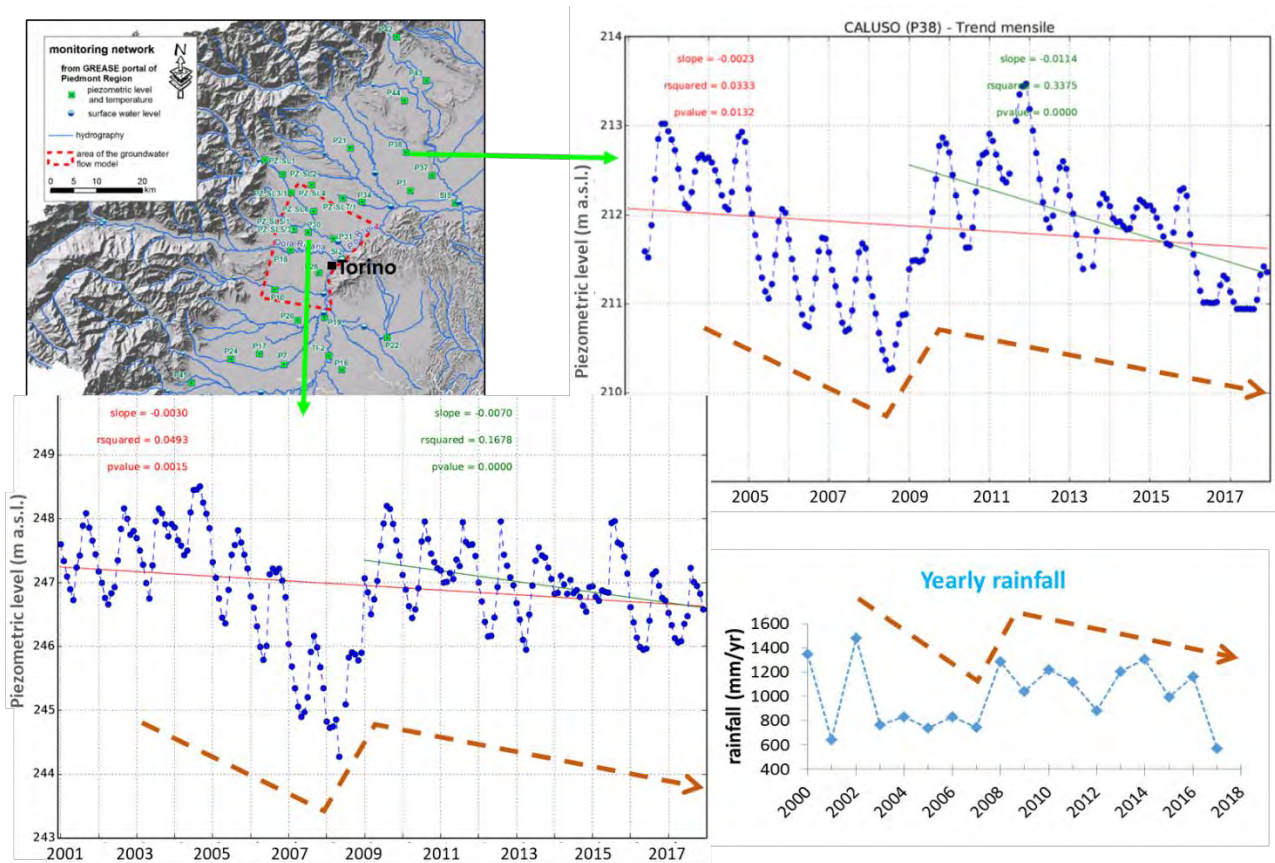


Fig. 2.13 –Piezometric levels evolution over the 2000-2017 period in two representative piezometers and comparison with the rainfall in the same period (the red and green continue lines into diagrams show the level trends over the period 2000-2009 and 2009-2017, respectively; the dashed arrows show schematically the patterns of piezometric heads and rainfall on the entire period).

As regards the chemical data, the trend analysis was focused on the Cl and NO₃ compounds in three area characterized by higher concentrations. The presence of high concentrations of these

chemical species has been taken as a reference of potential presence of anthropogenic impacts. The data processed for trend analysis belong to the monitoring wells listed in Tab. 2.3. The procedure followed for the trend analysis begins with a preliminary examination of data aimed at defining the statistical distribution frequency through the use of numerical tests and graphic elaborations (QQ-Plot, histograms, Box-Plot), followed by the identification and subsequent elimination of any outlier values (Dixon and Rosner tests). Once the dataset was redefined, the actual time analysis was performed with the Theil-Sen test. For each well the correlations between Cl and NO₃ were also checked. An example of this approach is shown in Fig. 2.14 where a clear positive correlation between chlorides and nitrates is observed.

zone	code	municipality	Address	aquifer	trend Cl	trend NO ₃
SCALENGHE	100200002	AIRASCA	Via della Moniga	CA	decreasing	decreasing
	126000001	SCALENGHE	c/o cimitero	CA	increasing	increasing
	126000004	SCALENGHE	Campo Prese	CA	increasing	increasing
	126000005	SCALENGHE	Campo Prese	PA	increasing	increasing
	126000006	SCALENGHE	Campo Sbarre	CA	increasing	increasing
	107100001	CERCENASCO	Strada Scalenghe	CA	increasing	increasing
POIRINO	105910001	CARMAGNOLA	Peso pubblico, P.za della Concordia	PA	insufficient	insufficient
	105900001	CARMAGNOLA	C.na Vigna	CA	insufficient	insufficient
	105910002	CARMAGNOLA	C/o Centro Sperimentale della Facolta di Agraria	PA	insufficient	decreasing
	105900004	CARMAGNOLA	Via Poirino Fraz. Casanova C.na Montebarco	CA	increasing	insufficient
	105900006	CARMAGNOLA	C.na San Pietro, Via Poirino 162	PA	insufficient	insufficient
	119710001	POIRINO	Parcheggio cimitero comunale, V.le delle Rimembranze	PA	insufficient	insufficient
	119700001	POIRINO	Via Covour/Str. Vecchia Poste	CA	insufficient	insufficient
	119700002	POIRINO	Fraz. Favari	CA	decreasing	decreasing
	119700003	POIRINO	Fraz. Ternavasso 11 bis - C.na Il Cavallino	PA	increasing	increasing
	119700008	POIRINO	C.na Bergera 25/1	CA	insufficient	insufficient
	119700009	POIRINO	Fraz. Marocchi - Via Tetto Nuovo 53	PA	insufficient	insufficient
	119700012	POIRINO	Tenuta Banna	CA	insufficient	insufficient
	119700015	POIRINO	C.na S. Croce 29	PA	insufficient	decreasing
	RIVOLI	109010001	COLLEGNO	Su strada in via della Piombia	PA	insufficient
109000002		COLLEGNO	Via Tampellini	CA	insufficient	decreasing
121900001		RIVOLI	Via Orsiera	CA	increasing	increasing
121900003		RIVOLI	Campofregoso	PA	increasing	insufficient
112000002		GRUGLIASCO	Fraz. San Rocco	CA	increasing	insufficient
102400003		BEINASCO	Destra Sangone	CA	insufficient	decreasing

Tab. 2.3 – Wells considered in the analysis of the time series, with indication of the results of the trend analysis.

QQ-Plots (Fig. 2.15) of Cl and NO₃ concentrations observed in the same well considered in Fig. 2.14 do not show an immediate connection to a Normal distribution. The Lilliefors and Shapiro-

Wilk tests also confirm the non-Normality of the data, as well as the non-referability to Log-normal or Gamma distributions.

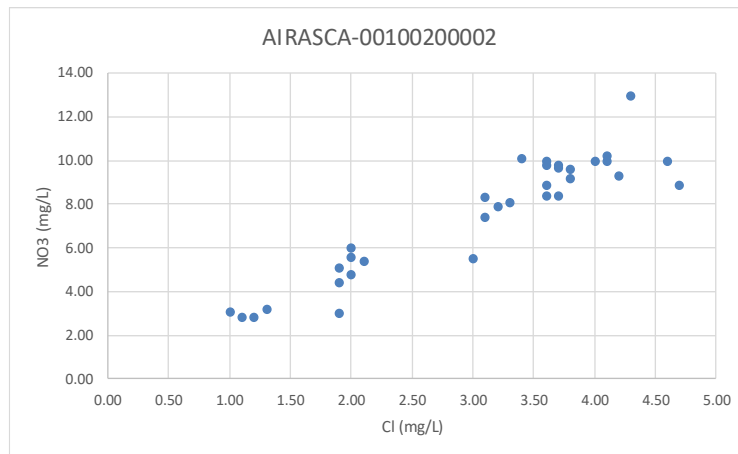


Fig. 2.14 – NO₃ versus Cl diagram. Data refers to AIRASCA monitoring well (code 00100200002).

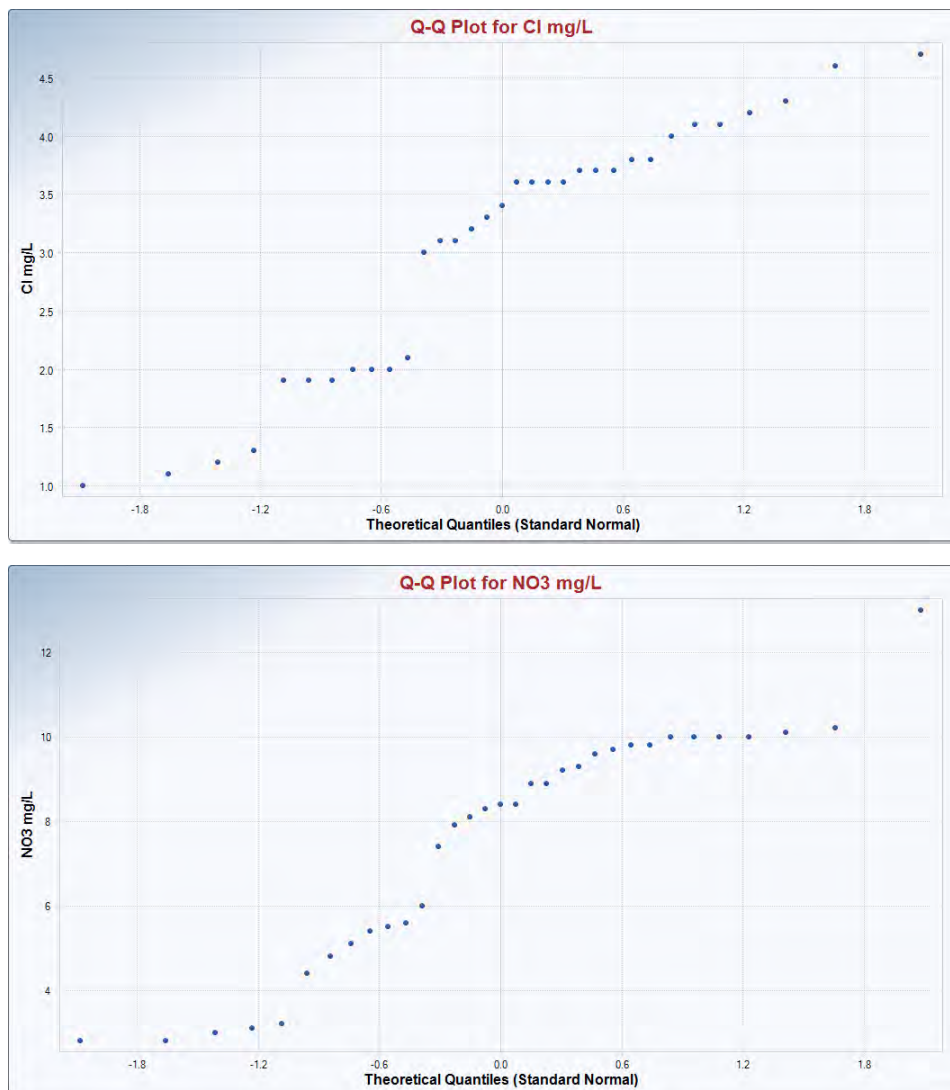


Fig. 2.15 – Q-Q-Plots of Chloride (up) and nitrate (down) concentration measured in the AIRASCA monitoring well.

The Dixon and Rosner tests showed the absence of outlier values for both data sets, therefore all the available data were considered in the trend analysis. Results are shown in graphical form in the diagrams of Fig. 2.16, where results of the Ordinary Least Square (OLS) Regression are also reported.

Both OLS Regression and the Theil-Sen Trend Analysis show the presence of a statistically significant decreasing trend over the period 2000-2017.

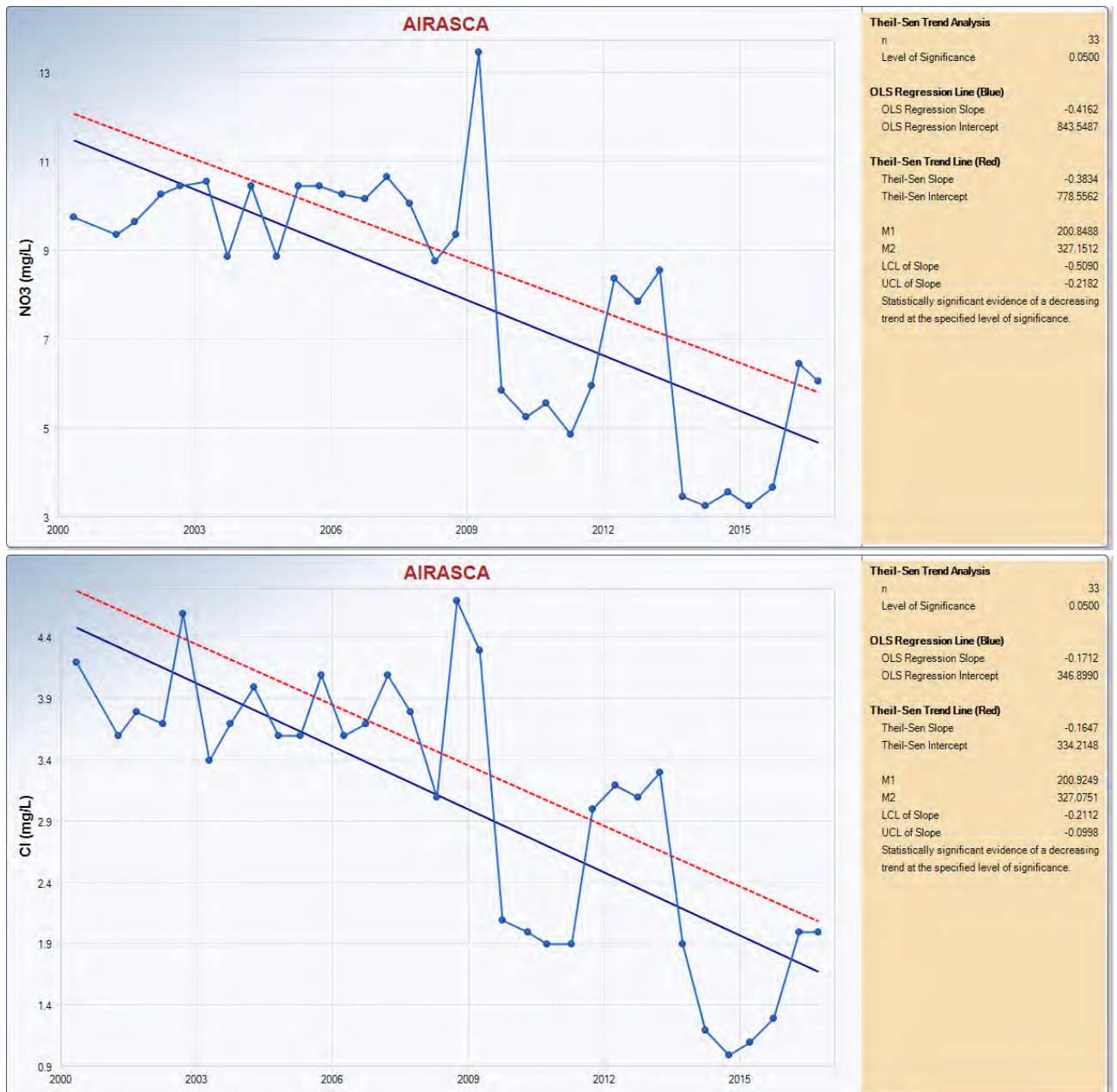


Fig. 2.16 – Time series of the NO₃ (up) and Cl concentrations (down) in the AIRASCA monitoring well. The dashed red line refers to Theil-Sen test, while the blue line refers to OLS Regression.

The same workflow was followed for all the other wells shown in Tab. 2.3, in which, as mentioned, the results of this analysis are also reported. Tab. 2.3 points out that the

SCALENGHE area is characterized by the greater critical issues with the presence of increasing trends both of Cl and NO₃ on all wells (excluding AIRASCA), with slope of the trend line always greater than 0.5. It is also important to underline that Cl and NO₃ contents are almost the same for CA and PA waters (Fig. 2.17), thus indicating a probable connection between the two aquifers and conditions of vulnerability also for the deeper aquifer.

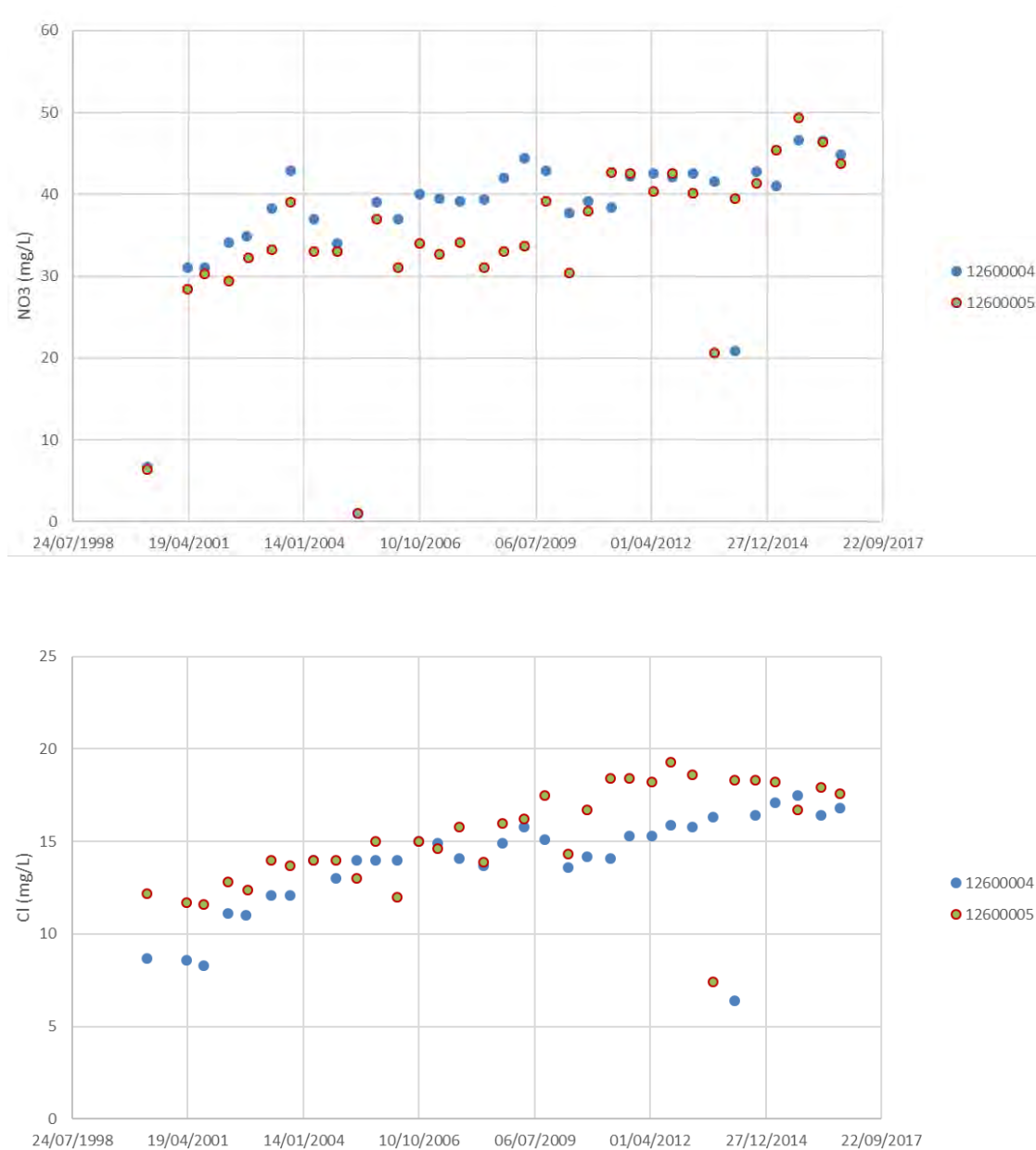


Fig. 2.17 – Chronograms of NO₃ (up) and Cl (down) concentrations measured in monitoring wells belonging to PA (code 0012600005) and CA (code 0012600004).

It is moreover important to underline as in the period 2009-2010 an abrupt increase of concentrations occurred in some wells and concurrently to the increase of rainfall and piezometric levels (Fig. 2.18). Hence, in that period a possible mobilization of salinity and nutrient accumulated in unsaturated zone during the dryer periods can be hypothesized. This

behavior confirms also in terms of water quality the sensitivity of the system to the hydro-climatic conditions.

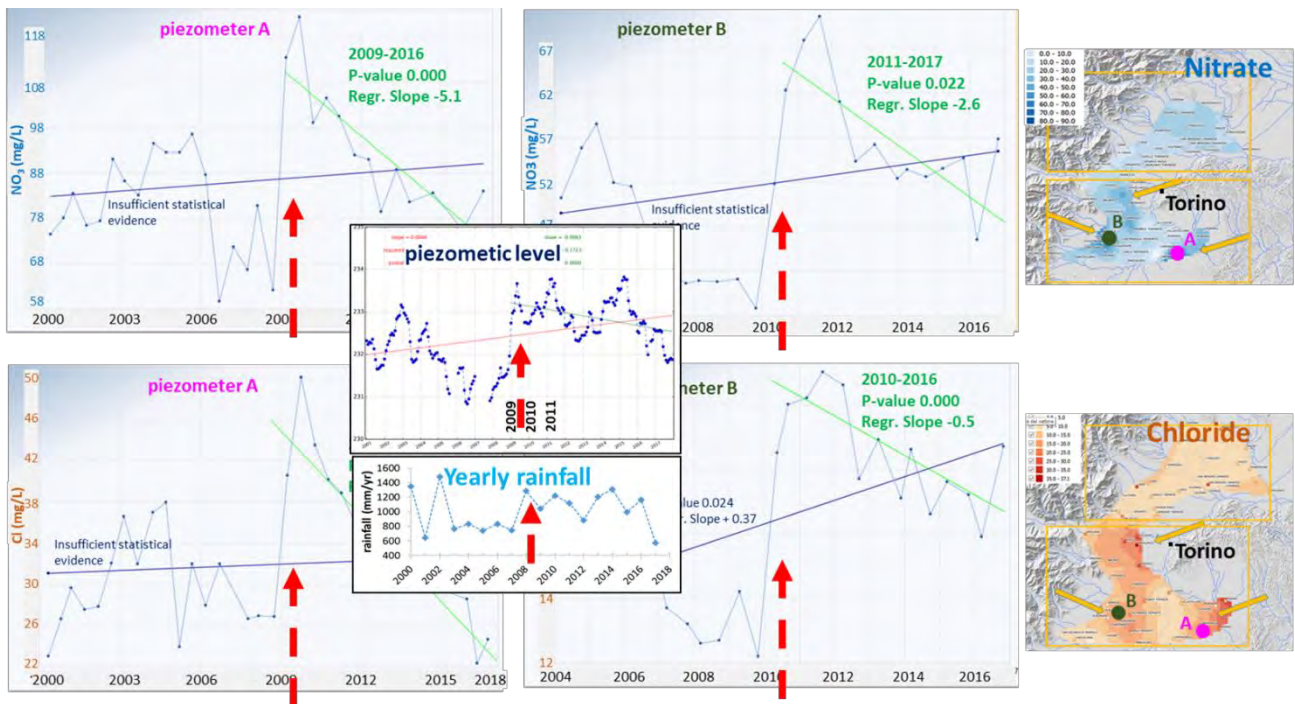


Fig. 2.18 – Chronograms of NO_3 (up) and Cl (down) concentrations measured in monitoring piezometers over the period 2000-2017 and comparison with piezometric levels and rainfall for the same period (the blue and green continue lines in the NO_3 and Cl diagrams represent the concentration trends over the periods 2000-2017 and 2010-2017, respectively; the red and green continue lines in the piezometric level diagram represent the level trends over the periods 2000-2017 and 2009-2017, respectively: the red dashed arrows evidence the moment of change for both chemical concentrations, piezometric level and rainfall).

3. PHYSICALLY-BASED GROUNDWATER FLOW MODEL OF THE FOOTHILL ALPINE AQUIFER SYSTEM

The model was developed within a sub-zone (Figs. 2.12 and 3.1) of the foothill Alpine aquifer system considered in the project. The zone consists in the foothill plain developed between the Western Alps and the Torino hill and it extends for a total of about 380 Km². It includes the Torino city and the neighbouring industrial and rural areas. Four important rivers flow in the study area: the Po, Stura di Lanzo, Dora Riparia, and Sangone rivers (Fig. 3.1). The choose of the model domain was performed according to the density of the piezometric level monitoring network, as well as basing on the data availability on geology, hydraulic parameters of the aquifer, pumping rates, etc.

Starting from the conceptual model of the aquifer previously discussed, the 3D numerical physically-based model was realized using the MODFLOW code (Harbaugh et al., 2000) and Visual MODFLOW as graphical user interface. This type of modeling is well appropriate for a porous aquifer, such as the aquifer system under study, and it enables verifying in a quantitative way the behavior of groundwater flow within the entire modeled space and under specific stresses, in terms of meteo-climatic conditions and/or exploitation rate and timing.

The model was before developed in steady state flow condition and then in transient flow condition. For the steady state conditions the average values over the period 2011-2015 were considered for the several parameters involved in the model. The transient state flow model was implemented and calibrated over the period 2011-2015, with 60 monthly stress periods and 10 time steps for each stress period.

3.1. Model implementation

In this sections, the main steps of the model implementation are summarized.

Active domain and spatial discretization

The active domain (Fig. 3.2a) was discretized horizontally with 100 rows and 100 columns with cells of about 200 m x 300 m. In order to represent the different aquifers of the system, 3 layers were implemented (Fig. 3.2b). The layer 1 is representative of the shallow phreatic aquifer and the layer 3 is the confined-semiconfined aquifer system. The layer 2 was used to implement the impermeable layer between the two aquifers, where it is present.

Hydrodynamic parameters

Initially, the hydraulic parameters (hydraulic conductivity, specific yield, specific storage) assigned to each cell were calculated considering the lithology, literature data, and some hydraulic tests performed in the area of interest. The values were then slightly modified during the calibration phase. Figure 3.3 shows for each layer and some sections the spatial discretization of the zone characterized by different hydraulic properties, whereas the Tab. 3.1 shows the values of the parameters in the previously mentioned zones.

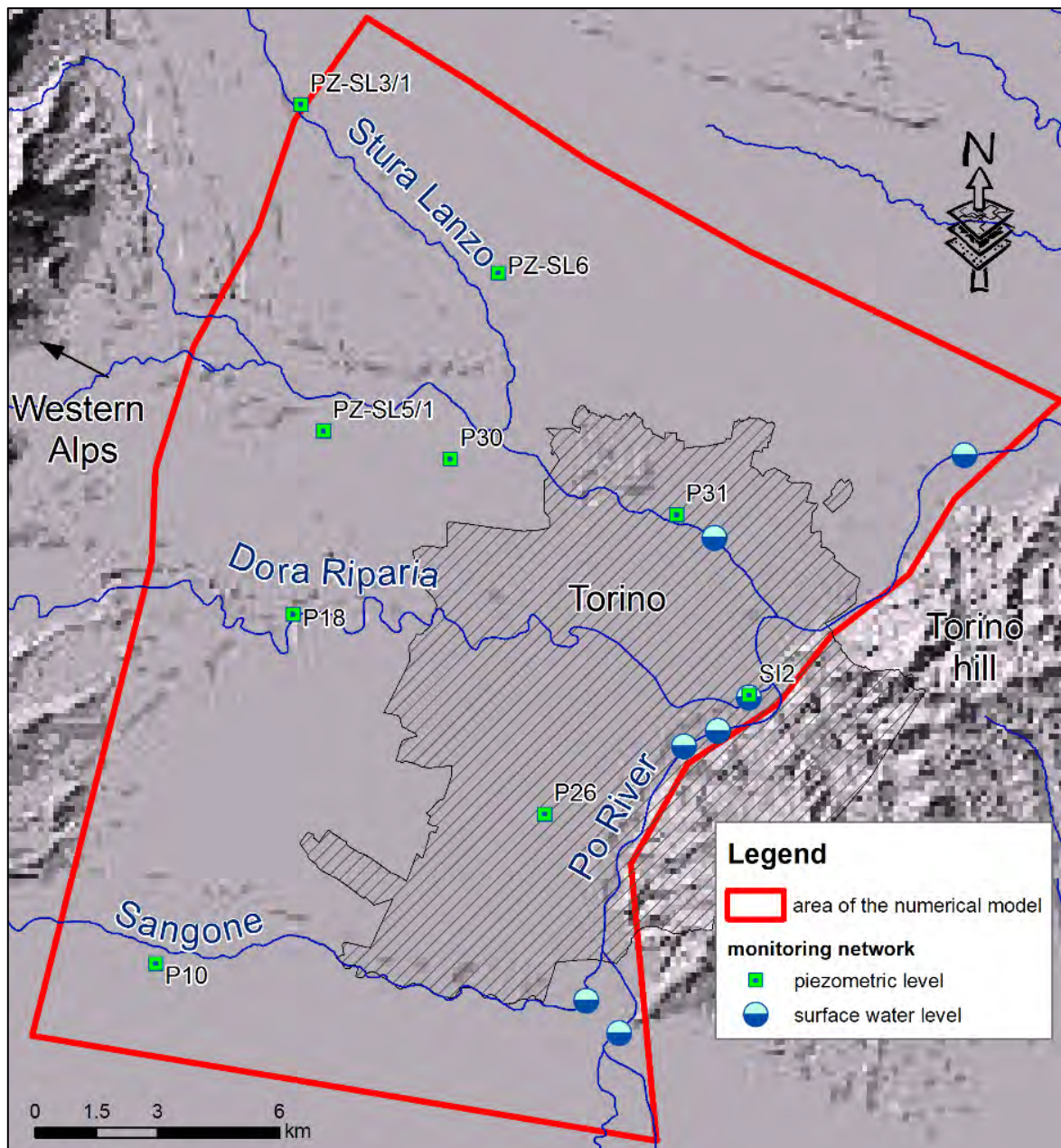


Fig. 3.1 – Area of the numerical model and monitoring network.

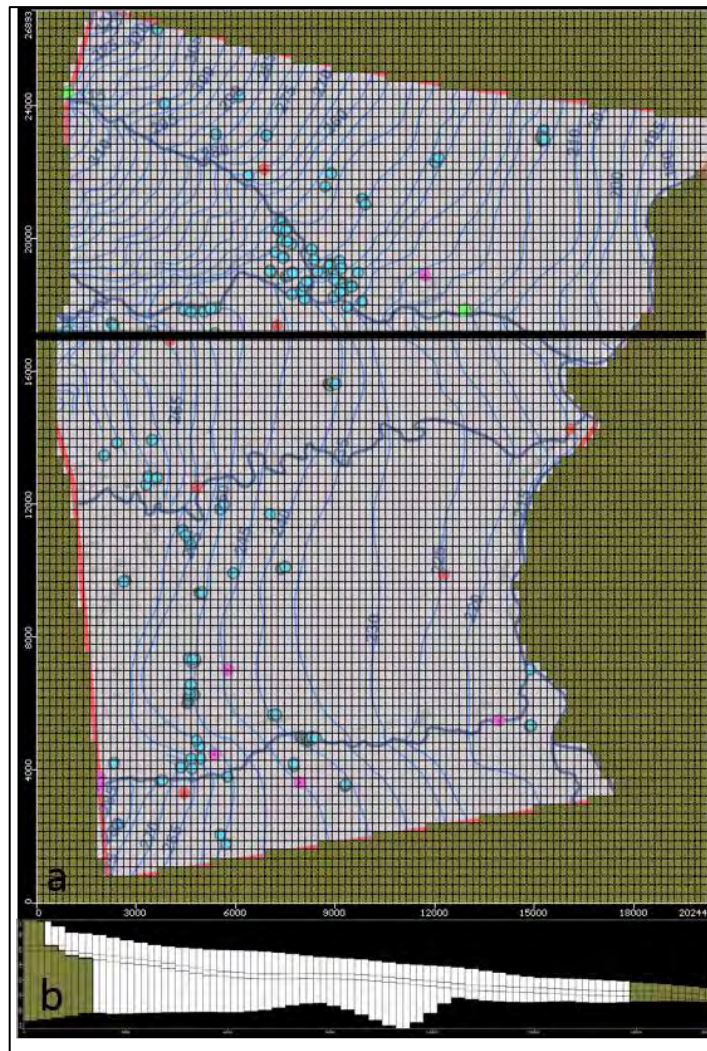


Fig. 3.2 – Spatial discretization in columns and rows (a) and layers (b). In the map are also reported the piezometric map (blue line), the drinking water wells (cyan circle) and monitoring stations (red, pink and green symbols). The ensemble of the white cells is the active zone of the model, whereas the brown cells are inactive.



Fig. 3.3 –Distribution of the zones accordingly to the different values of hydraulic parameters.

Zone	Kx=Ky (m/s)	Kz (m/s)	Ss (1/m)	Sy ()
1	0.0015	0.00015	0.0001	0.1
2	0.0025	0.0025		0.25
3	0.0005	0.0005		0.05
4	1.00E-06	1.00E-07	0.001	
5	0.0004	0.0004	0.0001	

Tab. 3.1 –Values of hydraulic parameters assigned to the different zones of the model.

Hydrologic boundary conditions

The Fig. 3.4 shows the boundary conditions of the model. Given its role of base level for the system, the Po river was implemented using a Constant Head (CH) boundary condition, whereas at the uppermost border, where the conceptual model indicates a feeding inflow component, a General Head Boundary (GHB) was applied. The others cells along the norther and southern boundaries were set as no-flow, because they cross perpendicularly the iso-piezometric curves.

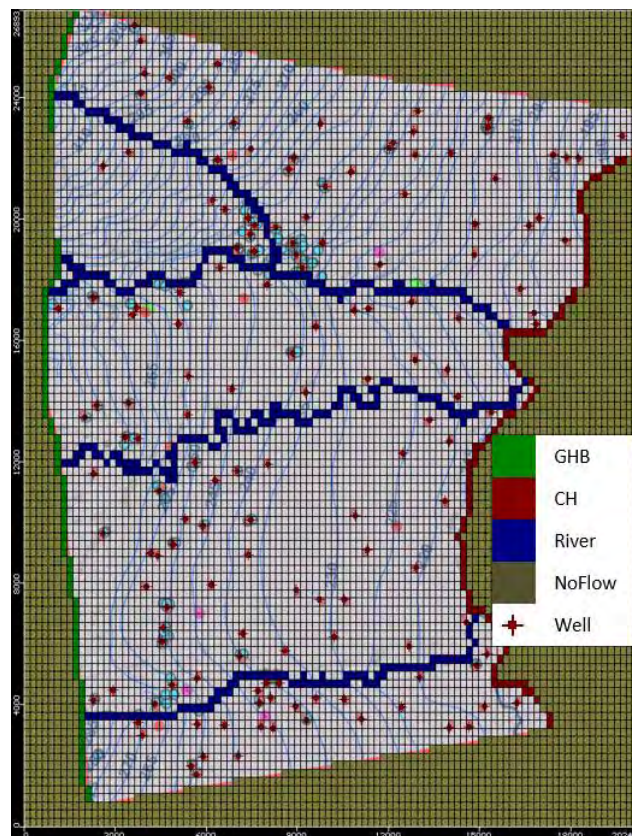


Fig. 3.4 –Boundary conditions.

The specified head of the CH was set basing on the data of 4 monitoring station of the Po hydrometric levels (Fig. 3.5), considering the annual mean value for the steady state model and the monthly values for the transient state model. For the GHB boundary condition, in the first model (steady-state condition) the used value of the specific head derived from the elaboration of the available piezometric map (Fig. 2.4). For the transient simulation, the hydraulic head in this boundary was varied considering the monthly variation in some monitoring station not included in the calibration phase (Fig. 3.5).

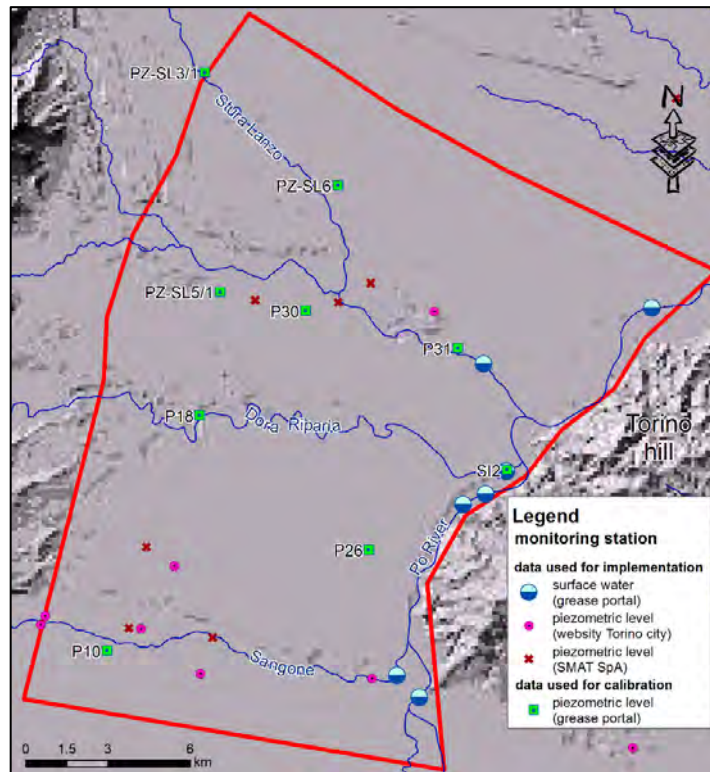


Fig. 3.5 –Monitoring stations whose data were used for the implementation and calibration phases.

Hydrologic sink and source terms

Recharge

The recharge values were achieved by applying infiltration coefficients to the effective rainfall. The latter derived from a soil hydrological model developed on a wider area in cooperation with the Politecnico of Turin, the ISAC-CNR and the SMAT-Ricerche, in the framework of a parallel study funded by SMAT. In particular, this hydrological model calculates the real evapotranspiration (AET) and the effective rainfall (ER), which represents the sum of runoff and groundwater recharge quantities. Considering the period 2011-2015, the annual and monthly mean values of these parameters for the specific zone of the groundwater model are shown in the Tabs. 3.2 and 3.3.

year	T _{mean} (°C)	Rainfall (mm)	AET (mm)	ER (mm)
2011	14.0	899	313	631
2012	13.5	682	311	448
2013	13.1	906	327	644
2014	14.0	1056	345	752
2015	14.2	778	339	528
mean	13.8	864	327	601

Tab. 3.2 – Annual mean value of temperature (T_{mean}), rainfall, real evapotranspiration (AET) and effective rainfall (ER).

month	T _{mean} (°C)	Rainfall (mm)	AET (mm)	ER (mm)
January	3.42	18	4	22
February	4.04	37	8	43
March	9.38	81	22	67
April	13.6	91	36	55
May	17.1	105	56	61
June	21.5	101	61	48
July	24.0	80	48	44
August	23.2	78	39	47
September	19.3	53	23	29
October	13.7	73	14	54
November	8.79	137	9	126
December	4.31	31	5	32

Tab. 3.3 – Monthly mean value of temperature (T_{mean}), rainfall, real evapotranspiration (AET) and effective rainfall (ER).

Infiltration coefficients of 30 % and 60 % were applied to the ER values respectively for urban areas and rural areas, thus achieving the recharge quantities.

These values were applied to the layer 1 by using the RECHARGE package. The total effective infiltration was 180 mm/year for urban area and 360 mm/year for rural area in the case of the steady state model. For the stress period of the transient simulation, the monthly values of effective infiltration for urban area (in red) and rural area (in green) are shown in the Fig. 3.6.

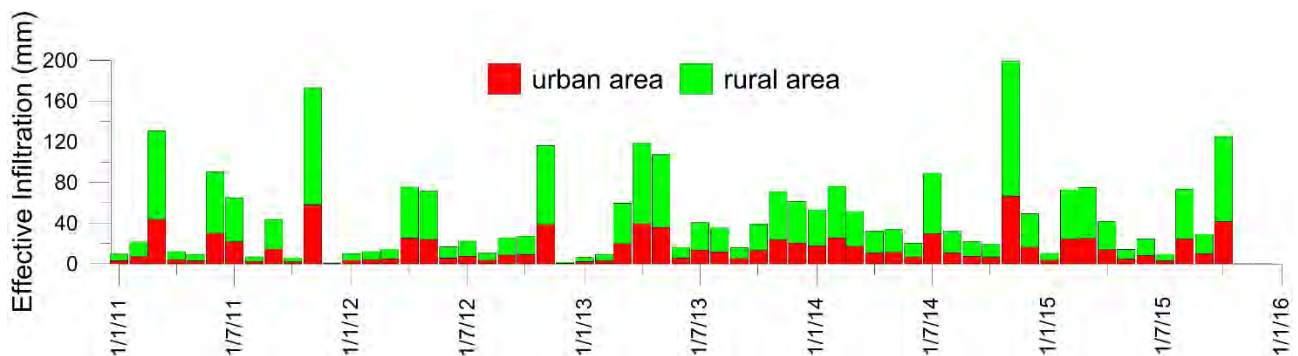


Fig. 3.6 –Effective Infiltration for urban and rural areas from January 2011 to December 2015.

Rivers

The main rivers (Sangone, Dora Riparia, Stura Lanzo) were implemented in the numerical model using the RIVER package (Fig. 3.4). The river head values (stage) come from the automatic station of the Grease Portal located in the area of interest (Fig. 3.5); the data of the LIDAR images were used for the values of the river bottom and width. The thickness of the riverbed sediment was set to 1 m and the initial value of hydraulic permeability of these sediments was set to one tenth of the value of the K_z of the zone 2 (Tab. 3.1). Subsequently, these values were slightly changed in the calibration phase.

Wells

Based on the available information, in the study area there are 168 wells for drinking water purposes and about 700 wells for other uses (domestic, agricultural, industrial, etc...) (Fig. 3.7). The amount of pumped water is not always known and there are a lot of uncertainty regards this information. The reliable data regard the monthly flowrate of the drinking water wells, which were provided by the water authority, SMAT SpA.

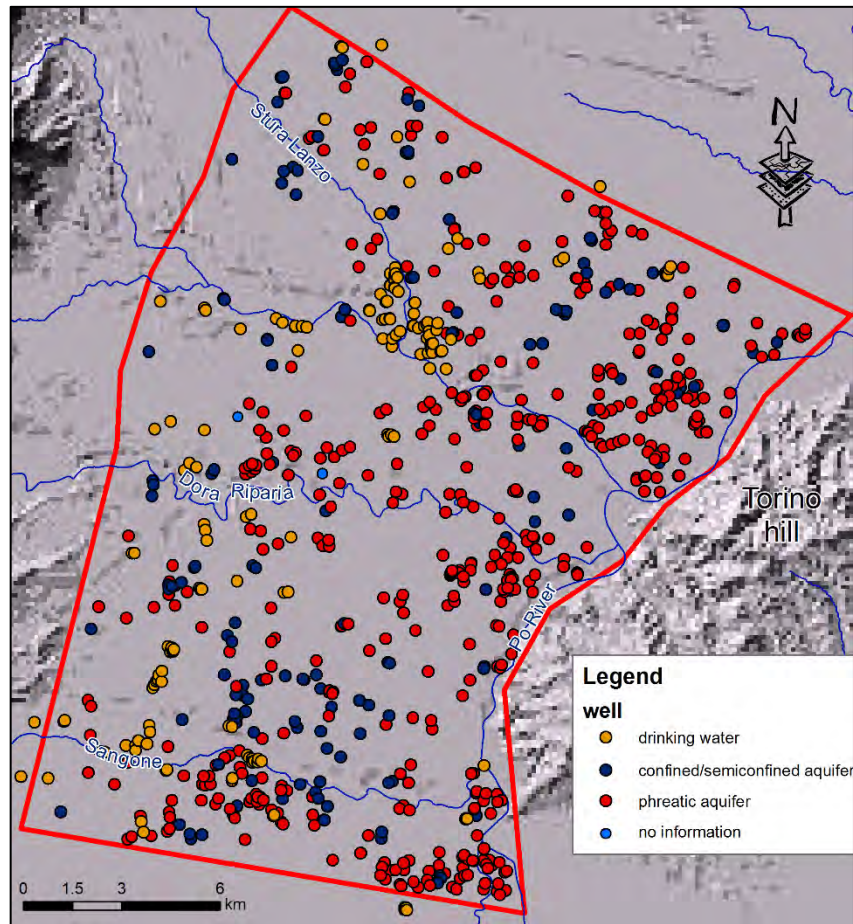
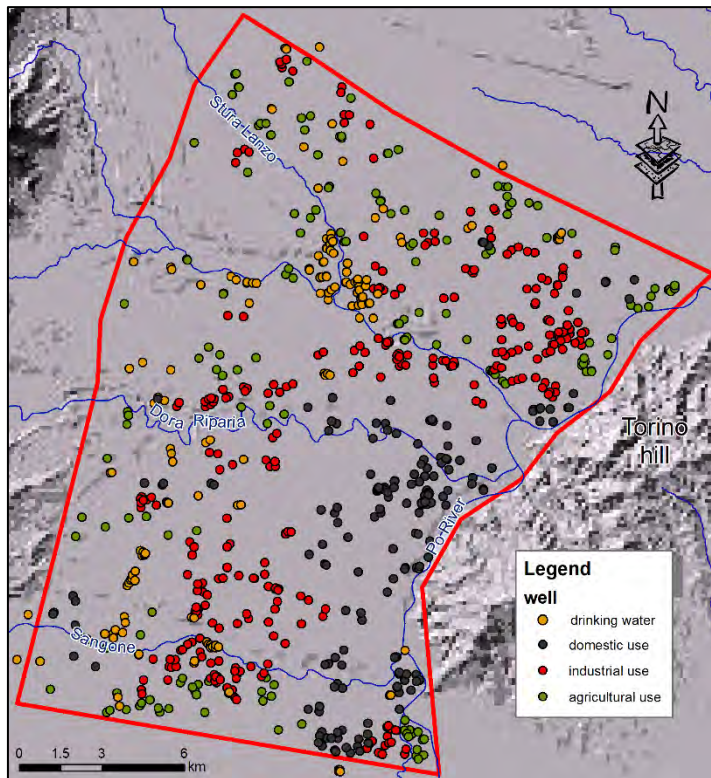


Fig. 3.7 – Drinking water wells and wells for other uses.

For the other wells a specific use was assigned basing on the land use (Fig. 3.8), thus obtaining 178 wells for agricultural purpose, 310 wells for industrial use, and 179 wells for domestic use. The annual amount of pumped water for each use was moreover estimated considering the “Piano Tutela delle Acque” (Regione Piemonte, 2007; 2018).



Well use	Total amount of pumped water (Mm ³ /year)
Drinking water	77
Industrial	66
Agricultural	11.5
Domestic	0.05

Fig. 3.8 –Distribution of the different use of wells in the area of interest and annual total amount of water pumped for different uses.

For the model implementation the wells of the same typology, similar depth and nearby located were grouped to obtain 57 drinking water wells groups, 43 industrial wells groups, 24 agricultural wells groups, and 26 domestic wells groups.

All the groups were simulated using the package WELL (Fig. 3.4), setting the total annual amount of pumped water distributed in 365 days, in case of the steady-state simulation, whereas for the transient simulation the different monthly flowrates (provided by the water authority or estimated) were inserted.

Initial condition

The initial condition of head for the steady-state was above the ground level, whereas the initial head for the transient state was the output of the calibrated steady-state model.

3.2. Model calibration and results

The used numerical solver is WHS solver with 50 outer iterations and 25 inner iterations. The Head change criterion (HCLOSE) and the Residual criterion (RCLOSE) were set to 0.01.

The objective of calibration is to identify a set of parameters that produce a satisfactory match between field observations and simulated values. The trial-and-error method was used to calibrate the model. Input parameters (mainly hydrodynamic and hydrologic parameters) were

adjusted within reasonable ranges in sequential run of the model until the model produce an acceptable match.

Figure 3.5 shows the 8 water head monitoring stations used for the calibration (Calibration Target). For the steady-state simulation the annual mean value was used, considering the data from January 2011 to December 2015. For the transient state the monthly values were used. Unfortunately, all the monitoring stations are representative of the phreatic aquifer, so it was possible to calibrate only the shallow aquifer. For the calibration of the deep aquifer some new monitoring station were installed by the water service (starting from January 2018) and, subsequently, will be used to calibrate also that aquifer.

As regard the calibration of steady-state simulation, in Fig. 3.9 are shown the observed vs simulated values of the calibration targets and the summary statistics. It is possible to note a good reliability of the model both for the morphology of piezometric map and for residual values (differences between calculated and observed value) that show a residual mean of 0.319 m, a standard error of 0.33 and a correlation coefficient of 0.999.

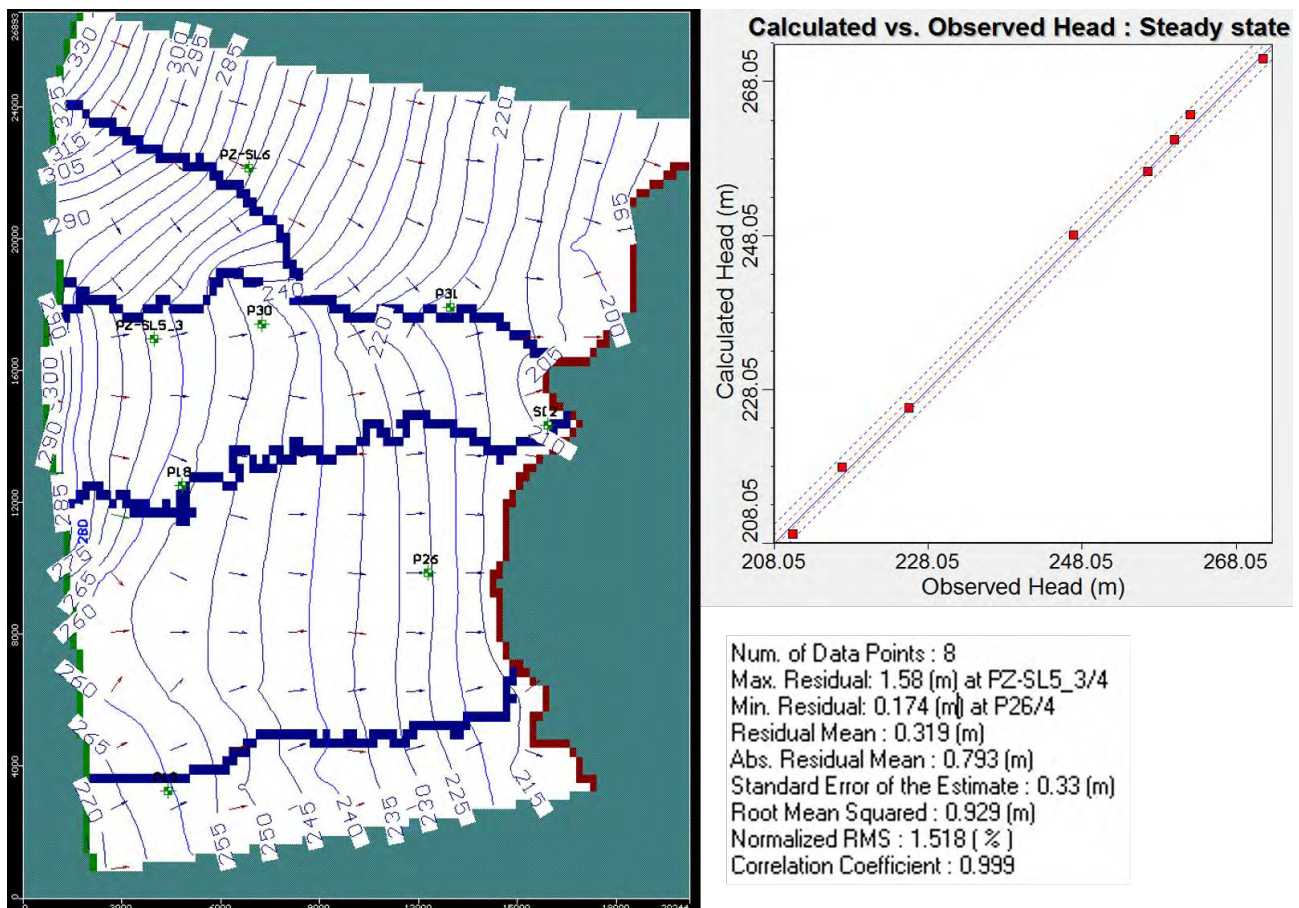


Fig. 3.9 – Water table elevation, observed vs calculated head graph, and statistic parameters of steady state model. In the map the location of calibration targets are shown (green symbols).

For the calibration of the transient state model, the monthly values of 7 monitoring stations were used (all those used for the steady state model, except the P31 station because it didn't record for the whole period).

In Fig. 3.10 some outputs of the transient state model referring to May 2015 (Time 1611 days) are shown as example: a piezometric map of the phreatic aquifer, a cross section with the flow paths, the observed vs calculated graph, the statistic parameters, and the water balance.

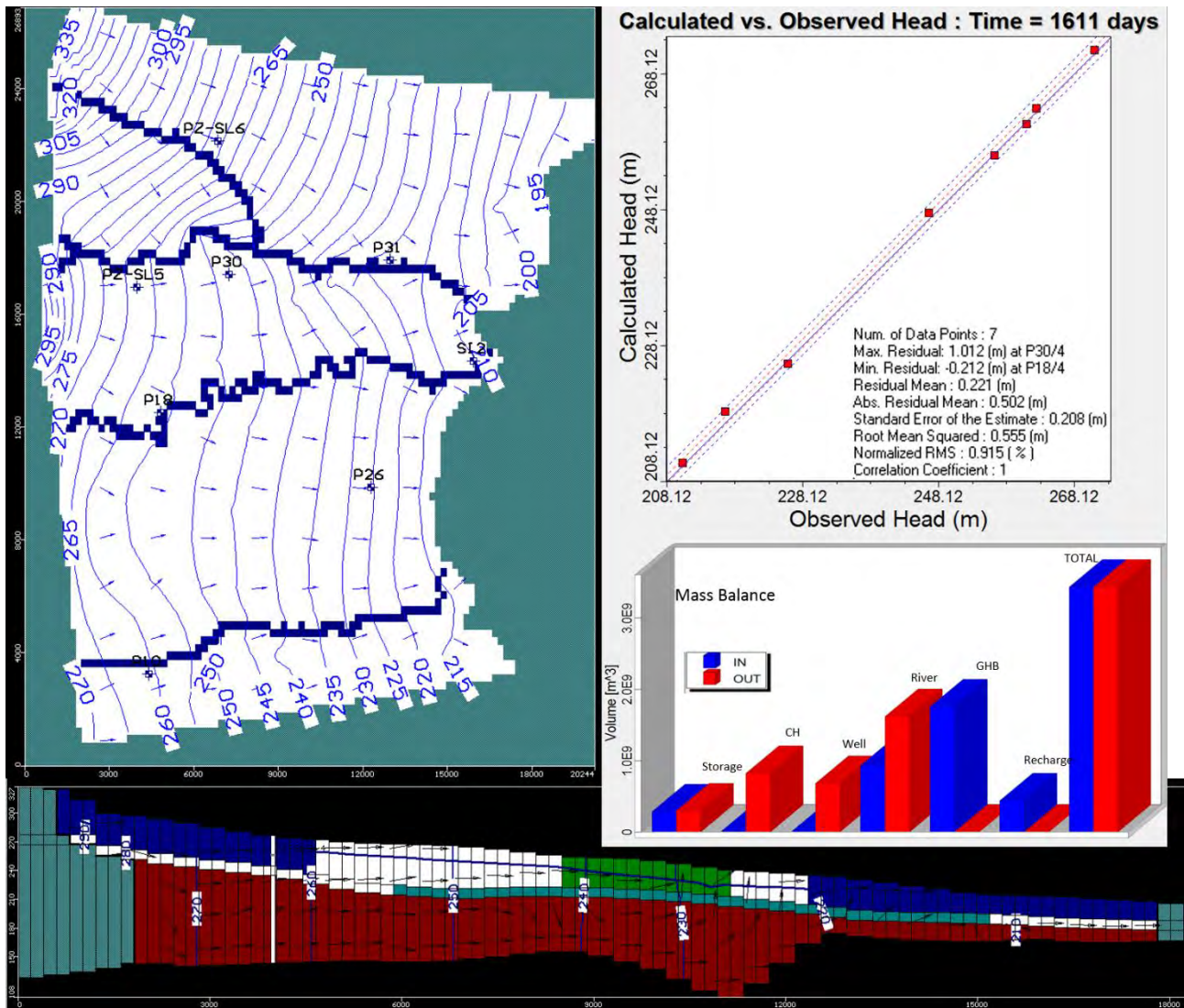


Fig. 3.10 – Piezometric map of phreatic aquifer, cross section with flow paths, observed vs calculated graph, statist parameters, and mass balance concerning May 2015.

The outputs of the model corroborate a good reliability of the numerical flow model and confirm, substantially, the conceptual model above discussed. In particular, the morphology of piezometric map is sufficiently congruent with that achieved in 2002 and the mass balance highlights that the main input to the systems are due to river seepage, transfers of groundwater that originate in upland zones, and local rainfall, instead, the outputs are for wells withdrawal and for river drainage. The good reliability of the model is also established by statistic parameters with a residual mean of 0.221 m, a standard error of 0.208 and a correlation coefficient of 1.

However, observing the variation over time of observed and calculated heads (Fig. 3.11), it is possible to note that in the central and southern zones the model is able to describe reliably the head variation (P18, P10, P26, SI2), whereas in north-western area (PZ-SL5, PZ-SL6, P30) the model not completely represent the head variation recorded in the monitoring stations. This could be tied to the presence of unknown variables that affect groundwater flow into the aquifer system (for example unknown withdrawal of wells for agricultural purposes, etc.). These areas should be object to further investigation and analyses to improve the conceptual model and, subsequently, the numerical model.

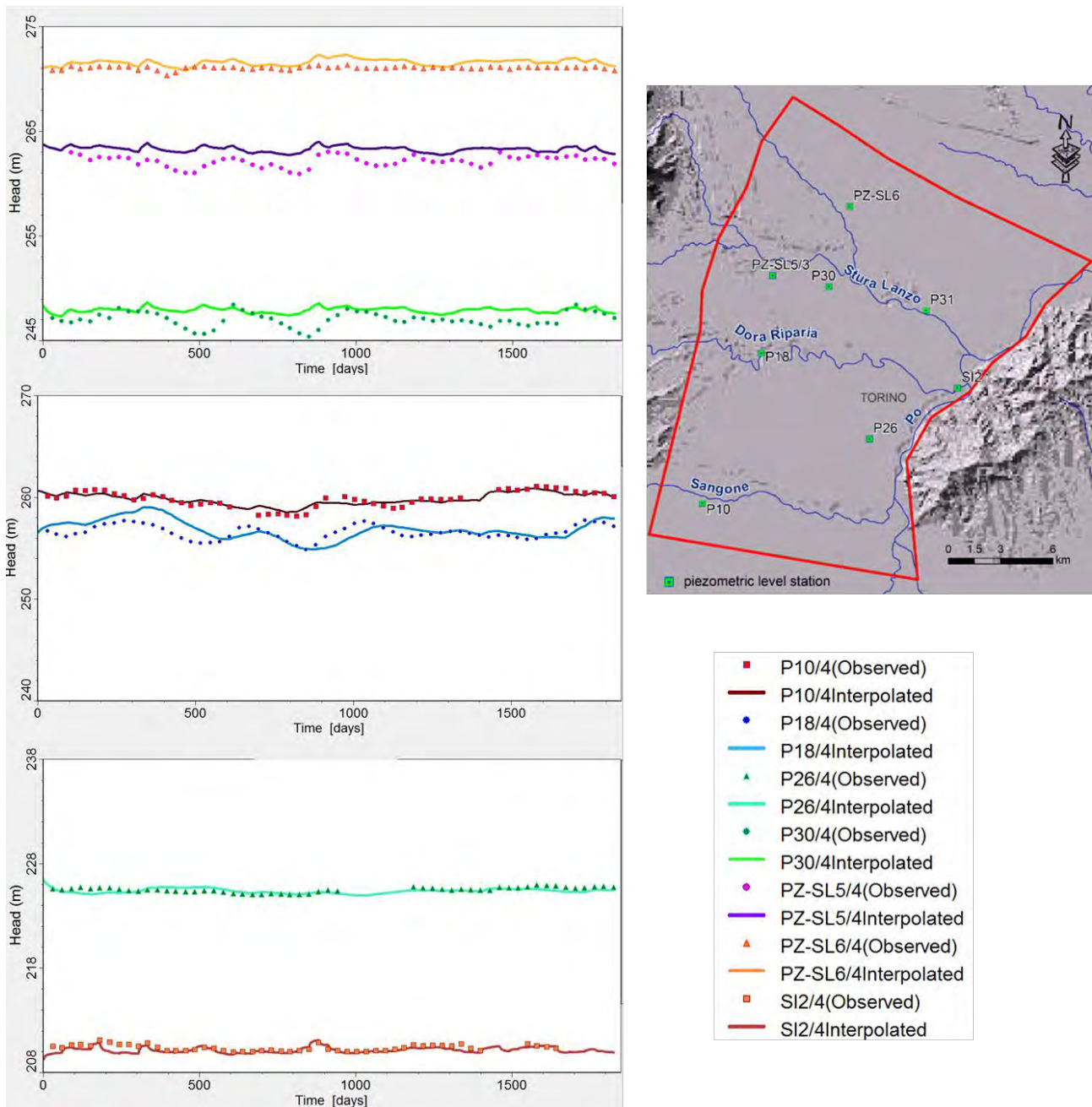


Fig. 3.11 – Comparison between observed and calculated water head for the target wells. In the map, the location of calibration targets is shown (green symbols).

3.3. Forecast simulation

Starting from the calibrated model, some forecast simulations were performed to verify the possible behavior of the aquifer system in response to expected changes regarding precipitation and temperature. For the estimation of meteorological data until December 2050, five available simulations of the RCA4 (Strandberg et al., 2014) driven by five different global models that provide the boundary condition for regional simulation (i.e. EC-Earth, CNRM-CM5, IPSL-CM5A-MR, HadGEM2-ES, MPI-ESM-LR) were analyzed. This choice enable obtaining a reasonably homogeneous ensemble of simulations at the local scale, but also representing the model uncertainty in the future projections captured by the different global models that drive the regional model.

These forecasted meteorological data were used as input data in the hydrological model developed by Brussolo et al. (2018), thus obtaining the value of real evapotranspiration (AET) and so the effective rainfall (ER). Among the hydrological available models, the MOHC-HadGEM2-ES was chosen because it was the only one characterized by a negative trend of ER, even if not statistically significant.

To such values of ER it was applied the calibrated potential infiltration coefficient of rural or urban area, thus obtaining the effective infiltration rate. The values of effective infiltration (2016-2050) were applied as recharge to the aquifer using the RECHARGE package at layer 1.

For all the others boundary conditions of the model (GHB, River, CH, Well), the monthly mean value of the calibrated period (2011-2015) were used. To obtain a more reliable forecast simulation it is advisable to develop also models aimed at estimating the variations of the boundary conditions (not foreseen in this project) according to the expected meteorological data (Menichini et al., 2016). However, as preliminary evaluation, in the figure 3.12 the results of the forecast model are shown for the piezometric levels of two representative wells (P10 and P26). The simulation confirms as the rate of local infiltration significantly affects the behavior of the piezometric head in the phreatic system. Moreover, a weak trend of decreasing of the piezometric levels is assessable, especially considering the second half period of the simulation.

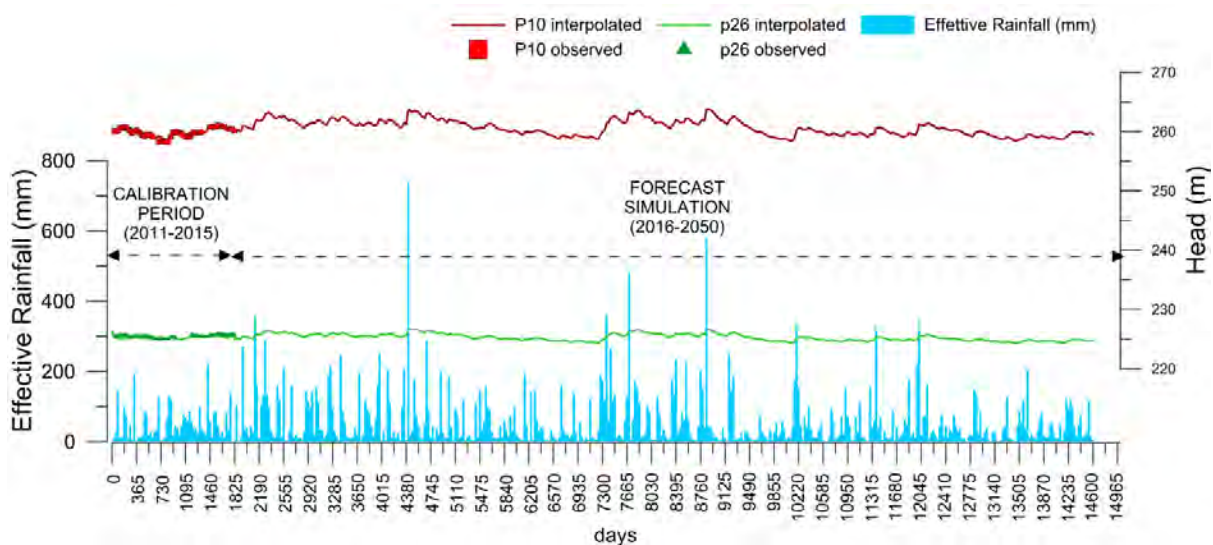


Fig. 3.12 – Forecasted water heads, regarding two selected wells (P10 and P26).

4. EMPIRICAL GROUNDWATER QUANTITY MODELS OF THE APPENNINES AQUIFER SYSTEMS

Empirical models were developed in order to numerically reproduce the flowrate evolution at selected strategic springs of the Apuan Alps and Mt. Amiata aquifer systems, whose conceptual models were widely discussed in the previous deliverable (D 1.2A). In particular, the modelling regarded the Galleria Nuova (GN in Fig. 4.1a) and the Cartaro springs (n. 13 in Fig. 4.1b), which represent the most important source of drinkable water (with some hundreds of L/s as average flowrate; see D 1.2A for more details) from the Mt Amiata volcanics aquifer and the Apuan Alps carbonate aquifer, respectively.

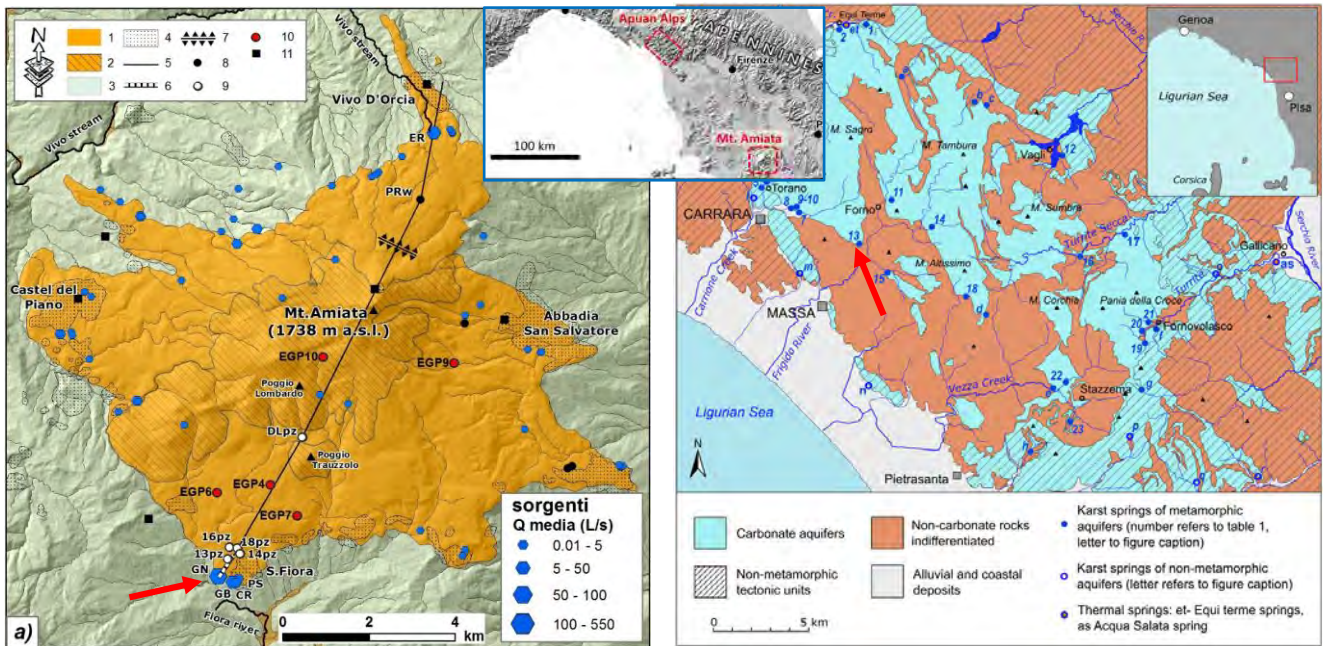


Fig. 4.1 – Hydrogeological sketch maps of the Mt. Amiata (on the left; from Doveri & Menichini, 2017) and Apuan Alps (on the right; from Doveri et al., 2018b). The red arrows indicate the location of the Galleria Nuova (GN) and Cartaro (13) springs, which were object of the empirical modelling.

A statistical analysis of the dataset was performed in order to find the relationships between the spring flowrate (Q) and the hydroclimatic parameters, such as rainfall (R), temperature (T), actual evapotranspiration (AE), effective rainfall (i.e. water availability, WA).

Two different software codes, ProUCL and Statistica 7, were used to investigate the frequency distribution of the data for the different parameters. These software codes were also employed to evaluate the main statistical parameters of the investigated variables and to process the data in order to build histograms, box plots and quantile-quantile plots (Q-Q plots).

Both Box-Whisker plots and an analytical process based on the Central Limit Theorem (Singh et al., 1997) were used to individuate potential outliers.

Time series Spectral Fourier Analysis (TSFA) were carried out on the variables in order to point out periodical events and to investigate the cause-effect phenomena between Q and meteorological data. Finally, a Multiple Linear Regression Analyses (MLRA) has been performed considering the Q as dependent variable and a function of water input (R and WA).

According to the specific hydrodynamic conditions of the aquifers (see D 1.2A), the statistical analysis and the modelling were performed on the base of monthly and daily values of the parameters, respectively for the Galleria Nuova spring (Mt. Amiata) and the Cartaro spring (Apuan Alps).

4.1. Flowrate model of the Galleria Nuova spring – Mt. Amiata aquifer

The data processing and the modelling have been performed referring to the period 1990 - 2017. The main statistical parameters of the monthly mean values of measured rainfall (R) and spring flowrate (Q) and calculated Water Availability (WA) are shown in Tab. 4.1, while the chronograms of the three investigated variables are reported in Fig. 4.2.

Variable	Valid N	Mean	Median	Minimum	Maximum	Variance	Std.Dev.	Coef.Var.	Skewness	Kurtosis
R (mm)	336	90.04	77.50	1.00	630	4239	65.11	72.31	2.56	14.44
Q (L/sec)	336	616	609	531	738	2838	53.27	8.65	0.77	-0.16
WA (mm)	336	45.02	15.50	0.00	592	4475	66.89	149	2.84	14.45

Tab. 4.1 – Descriptive statistics of R, Q and WA (WA was calculated according to Thornthwaite & Mather (1955), by combining monthly rainfall and temperature).

The figure shows a significant change in the patterns starting from 2009, especially in the case of the flowrate. In order to highlight statistical differences of the three studied variables, in Tab. 4.2 the main statistical parameters calculated before and after 2009 are reported, while in Fig. 4.3 the box-plots of each variable for pre- and post- 2009 are compared.

The comparison between pre and post 2009 dataset clearly shows that rainfall and water availability do not show statistically significant differences. The only dissimilarity between pre- and post-2009 is a higher number of extreme events with the consequent greater variability of post-2009 data. On the other hand, flowrate data show that pre and post 2009 values are significantly different.

As shown in Tab. 4.3, the investigated variables show the presence of potential outlier values following both Rosner's test and Box-plot diagrams. The potential outliers have been eliminated and data were reprocessed starting from the study of distribution; however, the frequency distribution does not change after elimination of outlier values.

Regression analysis can not be carried out if strong interrelationship of some independent variables are present. In this case, multi-collinearity appears making multiple Regression Model (MLR) inconsistent. In Tab. 4.4 the correlation matrix among all the accessible data has been reported. There is a statistically significant correlation between rainfall and water availability and between rainfall and air temperature. For this reason, only rainfall has been considered as independent variable in the regression model.

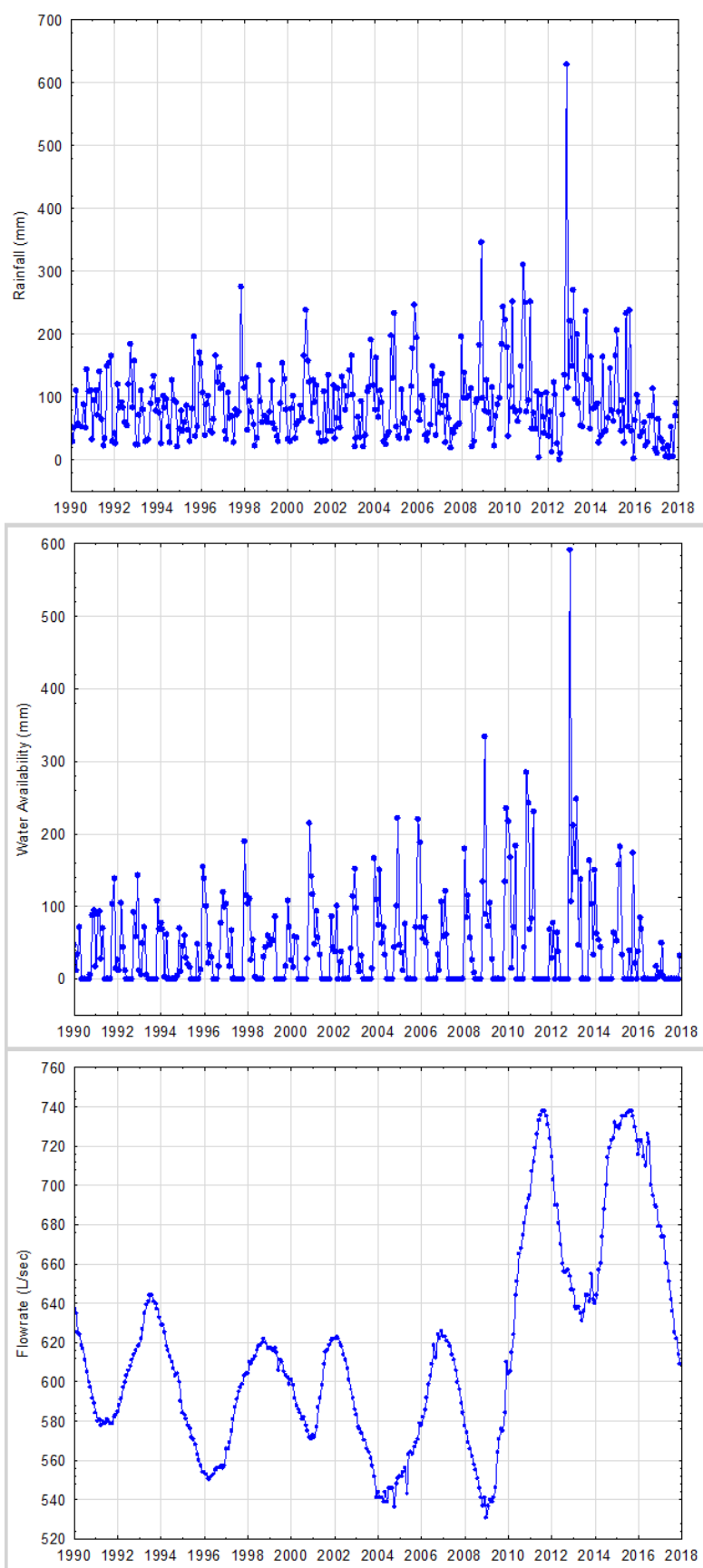


Fig. 4.2 – Chronograms of rainfall, water availability and flowrate of the Galleria Nuova spring, in the 1990-2017 period.

Variable	Valid N	Mean	Median	Minimum	Maximum	Variance	Std.Dev.	Coef.Var	Skewness	Kurtosis
R pre-2009	229	86.52	80.00	19.00	346	2672	51.69	59.74	1.32	2.95
R post-2009	108	97.56	76.50	1.00	630	7495	86.58	88.74	2.68	12.49
Q pre-2009	229	590	591	531	644	758	27.54	4.67	-0.14	-0.98
Q post-2009	108	669	674	531	738	3000	54.77	8.18	-0.72	-0.09
WA pre-2009	229	41.42	17.00	0.00	335	2897	53.82	130	1.77	4.30
WA post-2009	108	53.07	1.00	0.00	592	7762	88.10	166	2.90	12.55

Tab. 4.2 – Main statistical parameters pre- and post- 2009 of Rainfall (R), water availability (WA) and flowrate (Q).

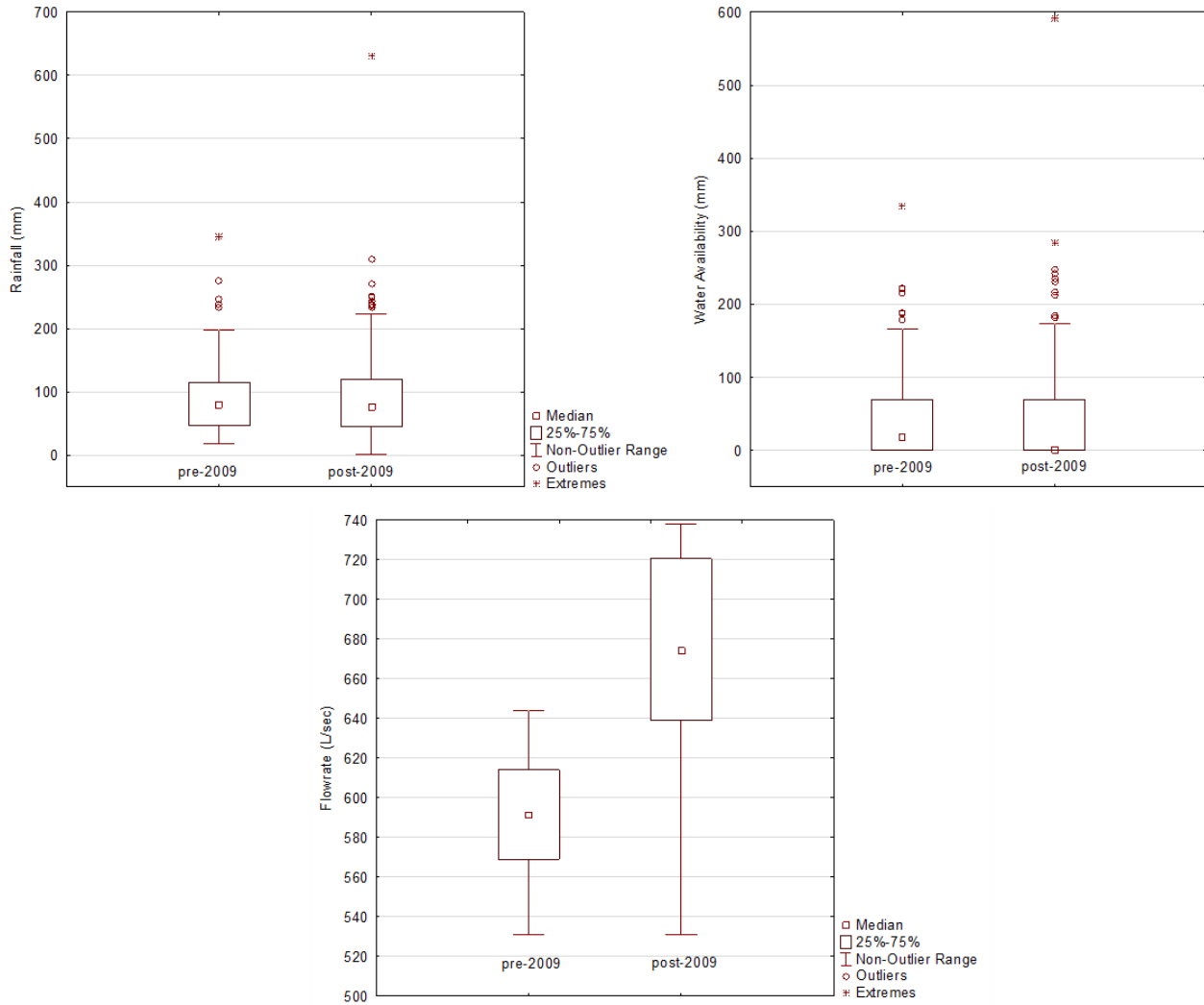


Fig. 4.3 – Box-plots of data pre-and post 2009 for each investigated variable.

Variable	Frequency distribution	Outlier (Rosner)	Outlier (Box-plot)
Rainfall	Gamma distribute at (0.05) Significance Level	3	12
Water availability	Data do not follow a Discernible Distribution (0.05)	3	17
Flowrate	Data do not follow a Discernible Distribution (0.05)	-	3

Tab. 4.3 – Results of frequency distribution test and outlier test.

	Means	Std.Dev.	Rainfall (mm)	Flowrate (L/sec)	Water availability (mm)	Air Temperature (°C)
Rainfall (mm)	90.02	65.14	1.000	-0.035	0.853	-0.272
Flowrate (L/sec)	615.6	53.28	-0.035	1.000	-0.043	0.027
Water availability (mm)	45.02	66.88	0.853	-0.043	1.000	-0.530
Air Temperature (°C)	11.30	6.166	-0.272	0.027	-0.530	1.000

Tab. 4.4 – Correlation matrix.

Time series are considered as the sum of many more simple time series, which have the form of regular sinusoidal (sine and cosine) functions, having different amplitude, wavelength and origin. In most case, TSFA is used to investigate electric engineering problems, where the signal is expressed in terms of frequency. On the other hand, from a geological point of view the wavelength and the required time for regularly repeating signal to exactly repeat itself (the period) appears to be more appropriate (Davis, 1986). Therefore, the periodogram was selected as graphical method to show spectral analysis, in which each single period is 1 hour (i.e. sampling interval).

The periodogram of TSFA performed on Rainfall and Flowrate showed that the main period for rainfall is N=12 months, while Flowrate shows a significant cycle at 56 months. Therefore, rainfall was smoothed by both 12 and 24 months moving average (R24), and the latter was selected for the regression modelling processing.

R24 and Flowrate(FR) are compared in Fig. 4.4 that shows an average delay time of about 24 months between the two parameters. For this reason, in order to maximize correlation between R24 and FR a shift of 24 lags has been applied on R24.

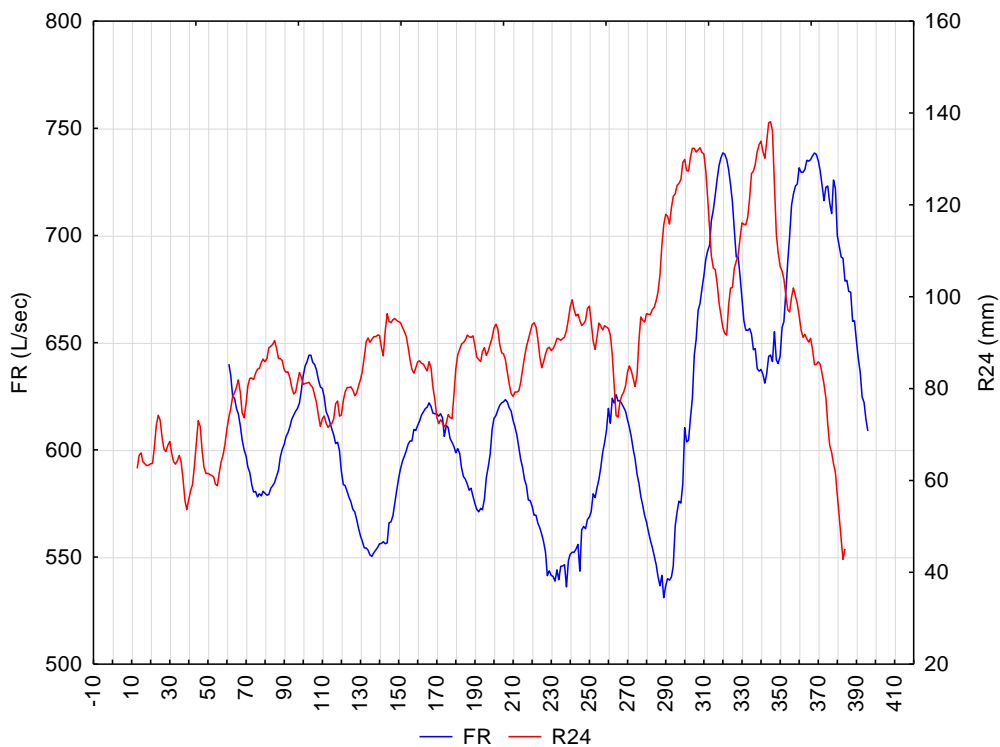


Fig. 4.4 – Chronograms of Rainfall moving average at 24 months (R24) and spring flowrate (FR).

A regression model has been achieved and results are reported in Tab. 4.5, where are inserted the standardized regression coefficients (b^*) and the raw regression coefficients (b). The magnitude of these *Beta* coefficients describes the dependence of FR on R24 independent variable. The *t*-value and resulting *p*-value are used to test the hypothesis that the intercept is equal to 0. The *Std. error* field contains the standard error of the intercept.

	b^*	Std.Err.	b	Std.Err.	t(298)	p-value
Intercept			349	11.42	30.59	0.00
R24 (mm)	0.81	0.03	2.86	0.12	23.83	0.00

Tab. 4.5 – Results of the regression modeling.

The equation of the regression model is therefore $FR=2.86 \cdot R24+349$.

In Fig. 4.5 the comparison between predicted and observed values is reported together with the ellipse that shows the prediction limit (at 95% interval of confidence) of the model for a single point and the regression line with prediction limits for this fitted line (at 95% interval of confidence). In Fig. 4.6 the observed and predicted flowrates are compared over time.

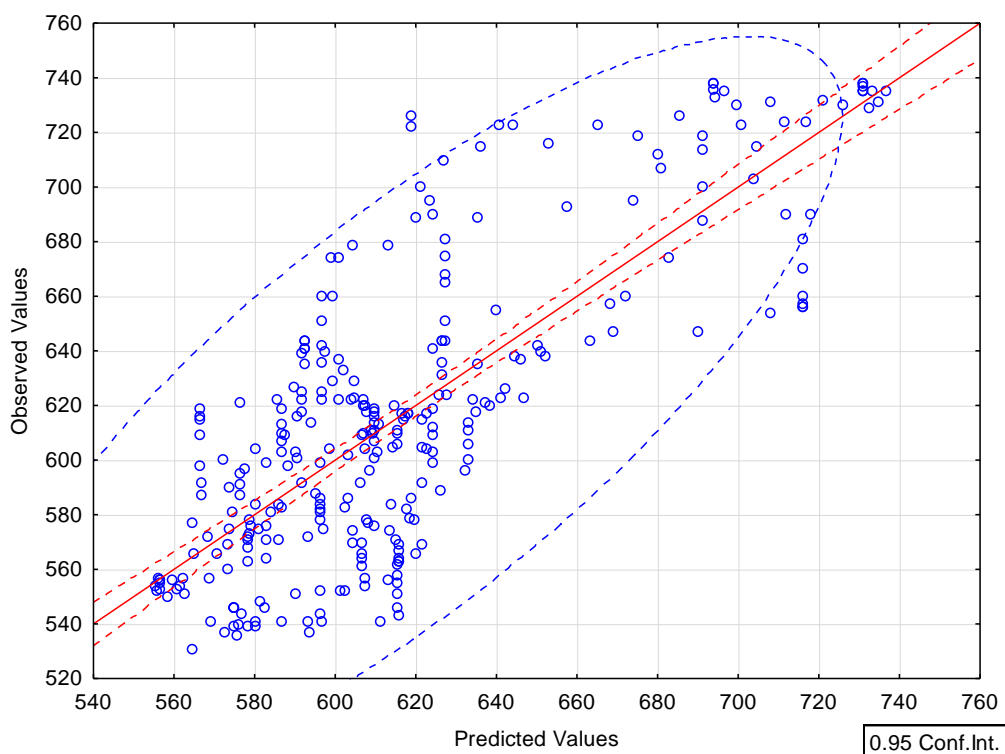


Fig. 4.5 – Predicted versus observed data.

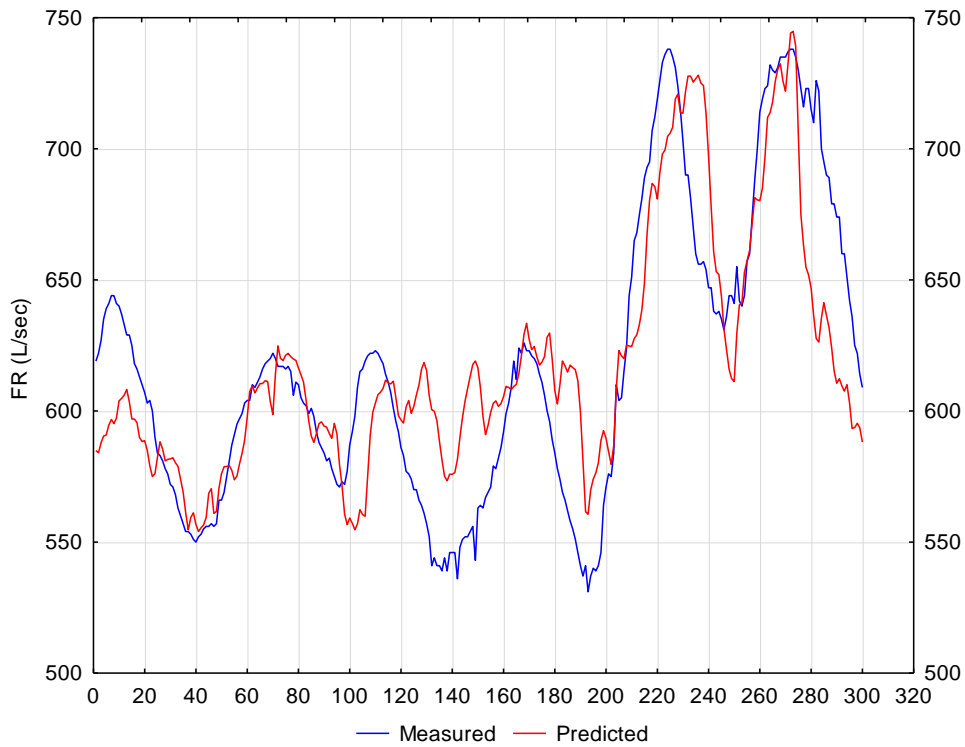


Fig. 4.6 – Time evolution of measured (blue) and predicted (red) FR.

Residual analysis allows evaluating the robustness of the model. As reported in Fig. 4.7 the residuals show a Normal distribution (Shapiro and Lilliefors test) and no outlier values are present (Rosner's test), thus pointing out the good robustness of the model.

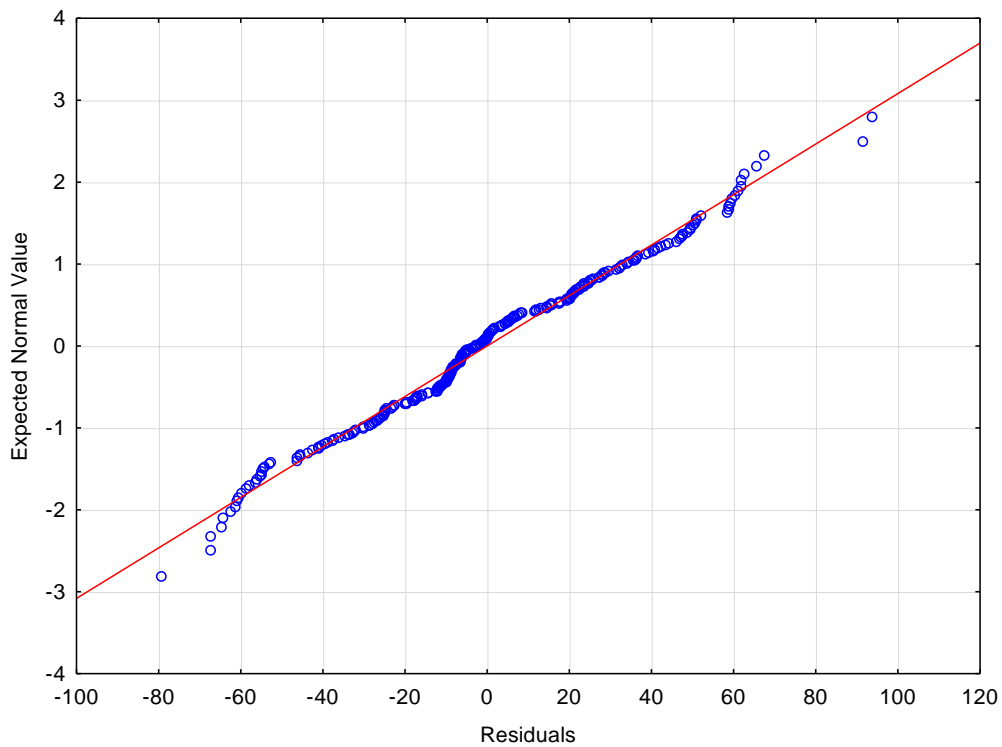


Fig. 4.7 – Daigram of Expected values of residuals assuming Normal distribution versus residuals values.

4.2. Flowrate model of the Cartaro spring – Apuan Alps aquifer

In order to develop a model able to reproduce the flowrate (Q) behaviour of the Cartaro spring respect to the weather conditions, a study of the historical series was performed on daily data of Q, air temperature (T), rainfall (R), actual evapotranspiration (AET) and water availability (WA). In order to obtain a regular sampling rate and make significant the series analysis, it was necessary to rearrange the flowrate data and estimate some values of this parameter. In fact, for some days no measures were recorded at the spring (16 days out of 6520) and in this cases the missing values were replaced by the average values between the flowrate recorded in the previous and successive days. The obtained continue time series was then subjected to a statistical analysis aimed at identifying possible outlier values. The study of data distribution and Q-Q plot and the application of the Rosner test showed outliers for values of $Q < 50$ and $Q > 500$. The 19 outlier values were replaced with the mean values between the adjacent points. Table 4.6 shows the main statistical parameters for raw and rearranged flowrate data, while in tab 4.7 the main statistical parameter of T and R are reported.

	Valid N	Mean	Median	Min.	Max	Lower	Upper	Variance	Std.Dev.	CV	Skewness	Kurtosis
Q [l/s]	6520	272.0	279.2	100.5	498.1	199.7	341.7	7411	86.09	31.65	-0.0706	-0.999
Qraw [l/s]	6486	298.4	279.2	49.00	104373	199.5	341.3	1853501	1361	456.3	70.85	5312

Tab. 4.6 Main statistical parameter of flowrate data before (Qraw) and after (Q) the reorganised processing,

Table 4.6 shows that the mean, the median and the interquartile interval have not significant variations between the two datasets, while it can be seen that the reorganization of the data results in a clear decrease in the standard deviation.

	Valid N	Mean	Median	Min.	Max.	Lower	Upper	Variance	Std.Dev.	CV	Skewness	Kurtosis
T (*C)	6520	11.8	11.6	-6.63	29.01	6.57	17.0	43.1	6.6	55.4	0.05	-0.83
R (mm)	6520	4.56	0.04	0.00	216	0.00	2.56	147	12.1	266	5.27	44.4

Tab 4.7 main statistical parameter of atmospheric temperature (T) and rainfall (R,)

The data processing and the modelling was performed referring to the period 2000 -2017, and focusing on the relationship between Q values and T and R values, The chronograms of the three investigated variables are reported in Fig. 4.8.

In Tab. 4.8 the correlation matrix among all the accessible data has been reported. Since there is not significant correlation between T and R, both have been considered in the regression model.

The periodgrams of TSFA performed on R, T and Q show the existence of cycles with six-months and annual periods. Therefore, rainfall and atmospheric temperature were smoothed by 30 days moving average (R30; T30). In order to better compare all variable and point out delay time, the same smoothing has been performed on flowrate (Q30).

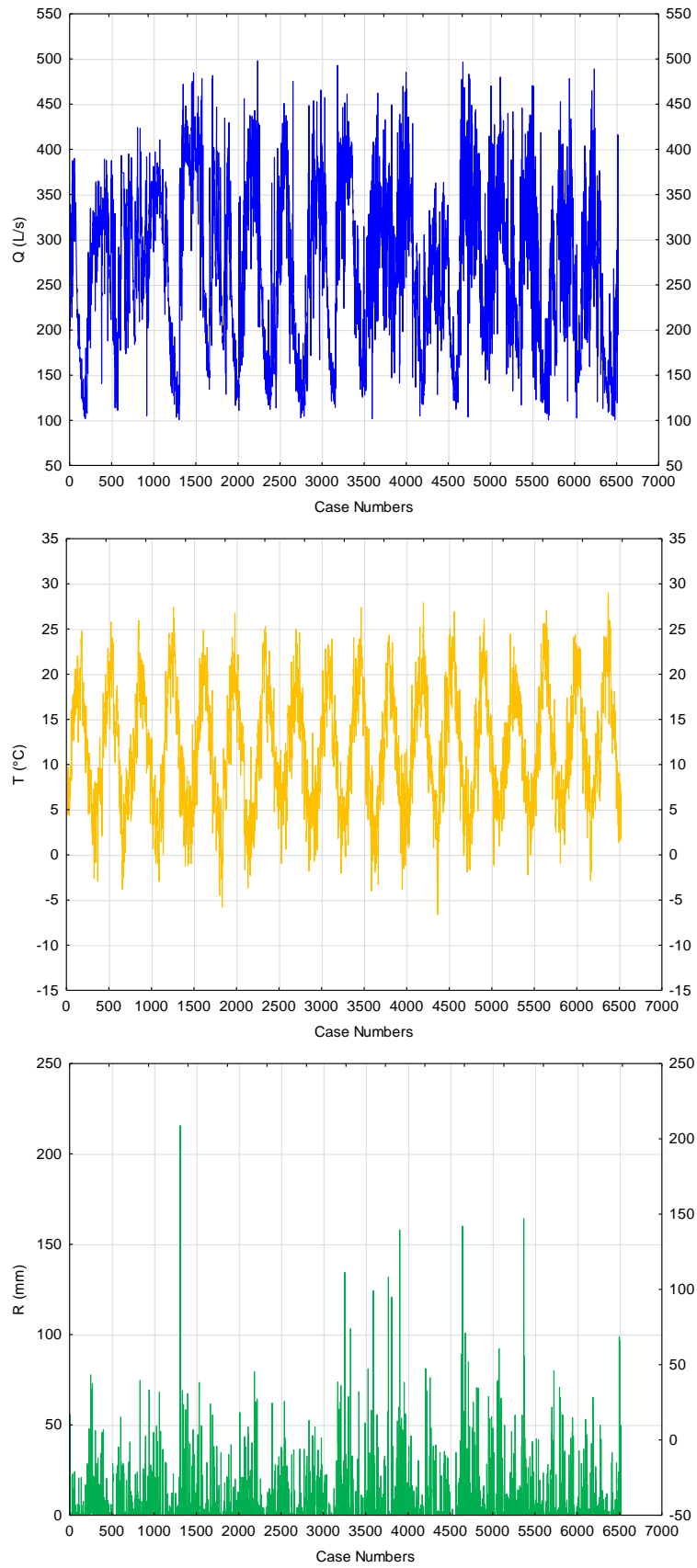


Fig. 4.8 – Chronograms of R, T and Q, in the 2000-2017 period.

	Means	Std.Dev.	T (°C)	R (mm)
T (°C)	11.8	6.56	1.00	-0.16
R (mm)	4.56	12.1	-0.16	1.00

Tab. 4.8 – Correlation matrix.

In the case of the T30 an average delay time of about 180 days was observed respect to the evolution of the Q30 (Fig. 4.9). For this reason, in order to maximize correlation between T30 and Q30 a shift of 180 lags has been applied on T30 (T30+180).

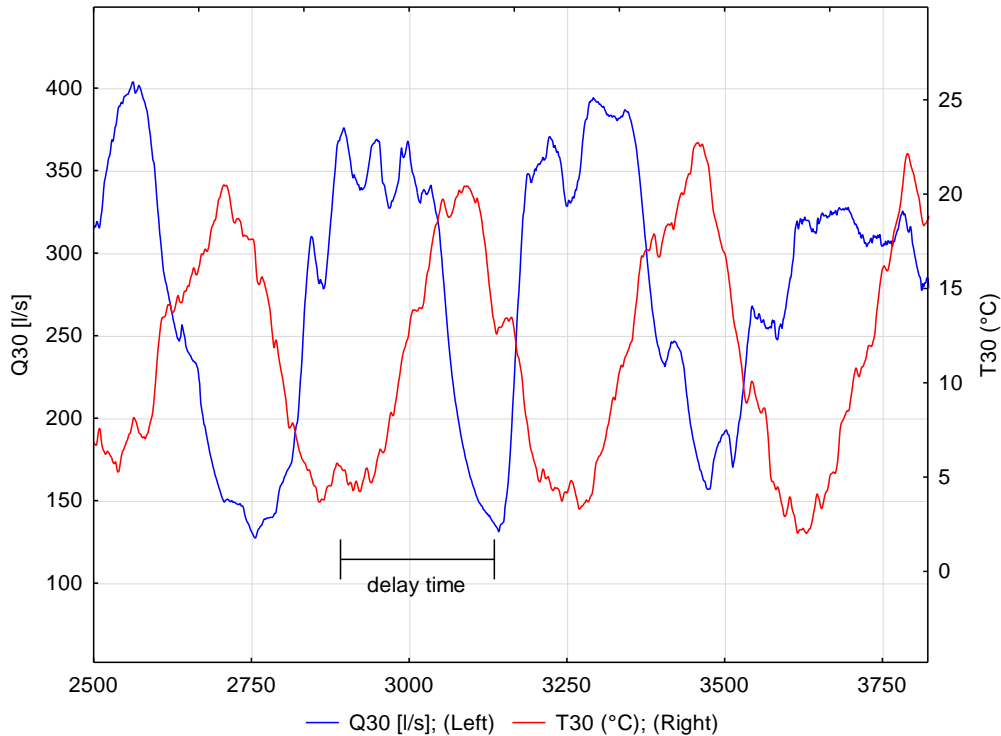


Fig. 4.9 – Chronograms of Rainfall moving average at 24 months (R24) and Flowrate (FR).

A regression model was finally achieved, thus linking the spring flowrate (Q) to the rainfall (R) and air temperature (T) by the following equation.

$$Q=3.1*R(30)+6.6*T(30+180)+181$$

Results are also reported in Tab. 4.9, where are inserted the standardized regression coefficients (b^*) and the raw regression coefficients (b). The magnitude of these *Beta* coefficients describes the relative contribution of each predictor to the overall prediction of the dependent variable. The *t*-value and resulting *p*-value are used to test the hypothesis that the intercept is equal to 0. The *Std. error* field contains the standard error of the intercept.

	b^*	Std.Err.	b	Std.Err.	t(6307)	p-value
Intercept	-	-	181.4	2.091	86.760	0.000
R(30)	0.1347	0.011550	3.10	0.27	11.67	0.000
T(30+180)	0.4599	0.011550	6.62	0.17	39.82	0.000

Tab. 4.9 – Results of the regression modeling.

In Fig. 4.10 the comparison between predicted and observed values is reported together with the ellipse that shows the prediction limit (at 95% interval of confidence) of the model for a single point and the regression line with prediction limits for this fitted line (at 95% interval of confidence). In Fig. 4.11 the observed and predicted flowrates are compared over time.

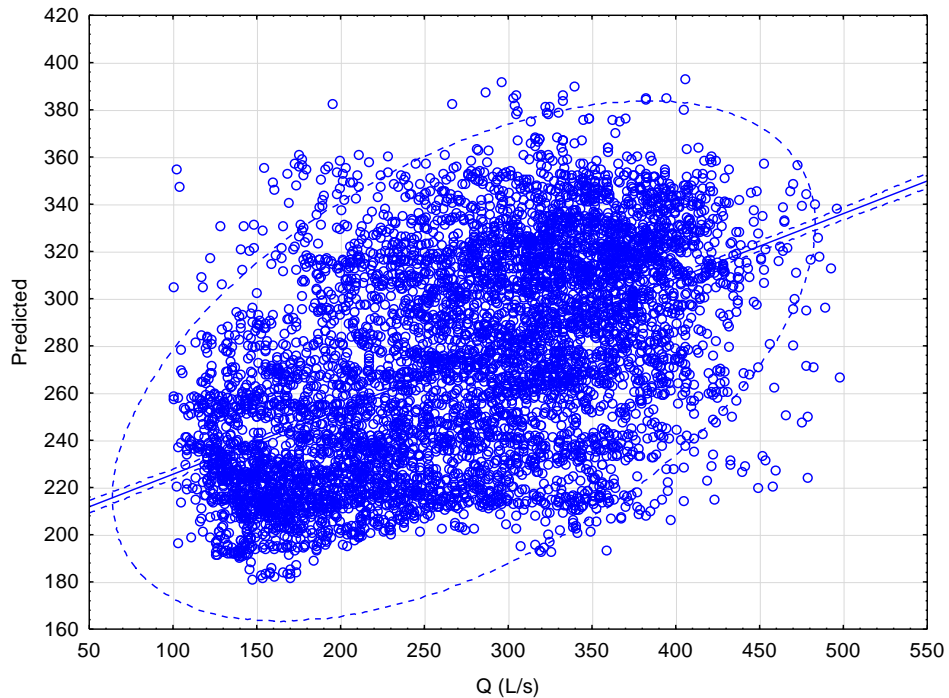


Fig. 4.10 – Predicted versus observed data.

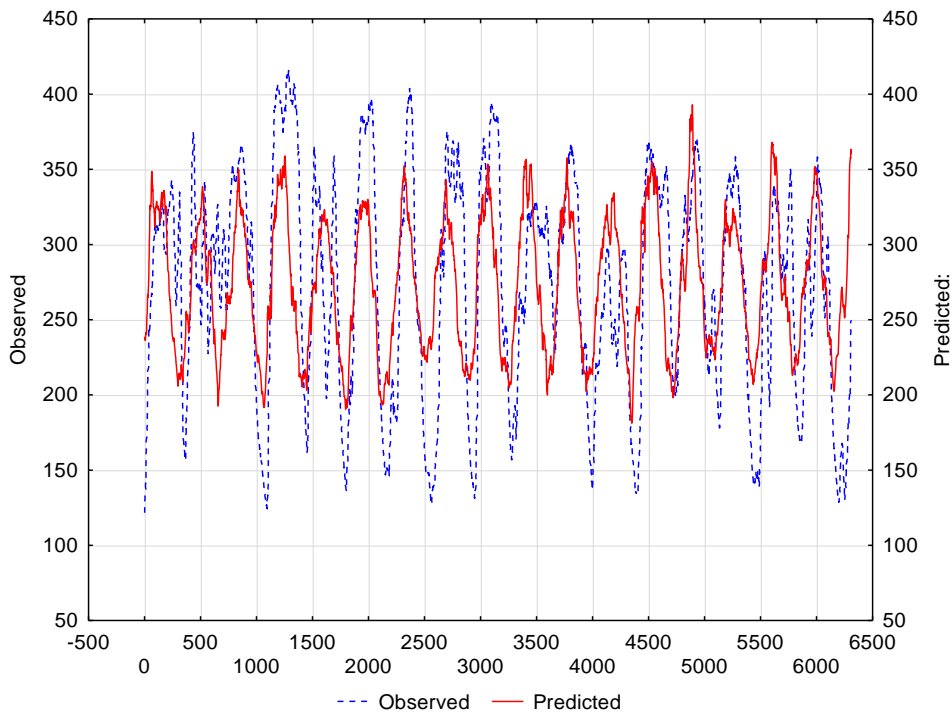


Fig. 4.11 – Time evolution of measured (blue) and predicted (red) Q.

The figure shows that the model has a good approximation of the trend shown by the measured values, even if it overestimates the lowest values and sometimes underestimates the highest values of flowrate.

Residual analysis allows evaluating the robustness of the model. In Fig. 4.12 and in Fig. 4.13 the histogram and the Normal probability plot of standard residual are reported.

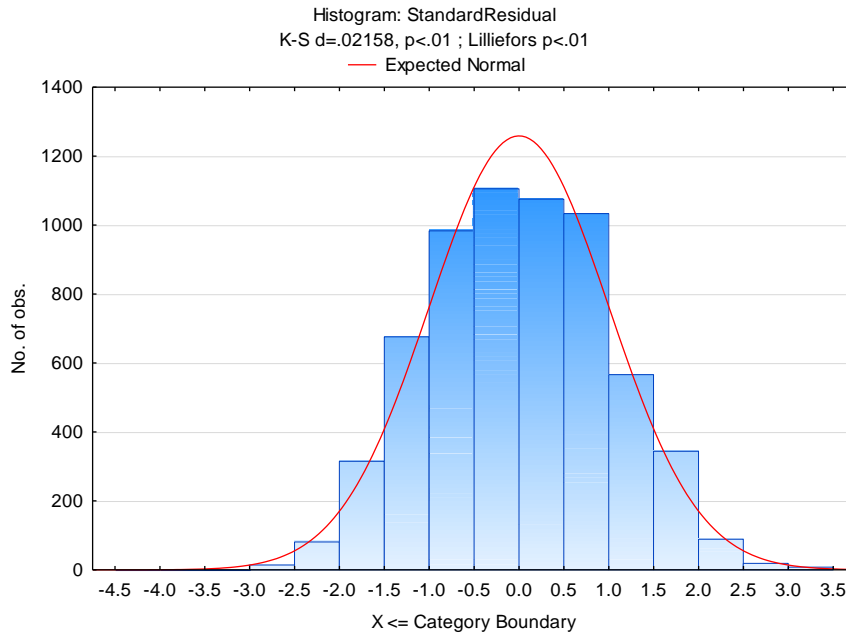


Fig. 4.12 – histogram of standard residual

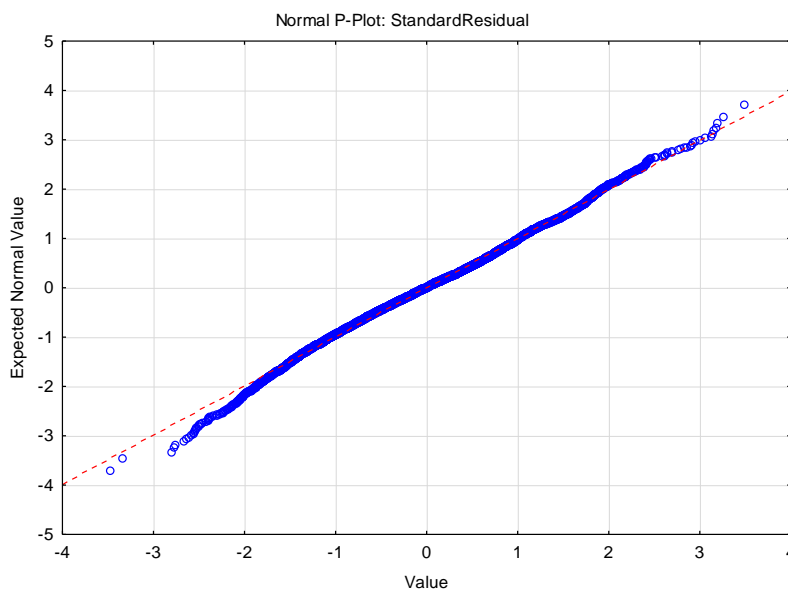


Fig. 4.13 – Normal probability plot of standard residual

These diagrams show that the frequency distribution of the residual values is approximate Normal. Moreover, if we consider the regression model reliable when the uncertainty on the predicted values (evaluated as standard deviation) falls in the range $\pm 2\sigma$, we can conclude that the developed model explains about 80% of the observed variance.

5. CONCLUSION

This deliverable concludes the activities of the Task 1 of the WP 1.2, providing the conceptual model of the foothill aquifer system of the Alpine area and the numerical models for the three aquifers systems involved in the project (the same foothill system and the two Apennines systems, in the Apuan Alps and Mt. Amiata areas).

The foothill aquifer results deeply affected by the hydro-climatic conditions of the Alpine range, because its groundwater flow is mainly fed by seepage from stream water originating in mountain catchments and by lateral transfers of groundwater that originate in upland zones. The significant sensitivity of the aquifer towards the meteo-climatic variations and changes is well pointed out by the piezometric heads evolution, as well as by the associated effects on the groundwater chemical features.

As regards the numerical models of groundwater quantities, these were developed for the three systems (Apuan Alps, Mt. Amiata and foothill Alpine aquifers) through different approaches, which were steered by the respective conceptual models. For the Alpine foothill aquifer, a physically-based model has been implemented and calibrated over a wide area, thus quantifying the several terms of the groundwater budget, as well as their evolution along time. Empirical regression models were instead elaborated by a statistical approach for reproducing the flowrates evolution of two main springs, which are fed by aquifers of the Apuan Alps and Mt. Amiata, respectively.

The models represent a valid tool for forecasting the possible evolution of groundwater yield under expected weather and climate conditions.

Generally speaking, the work performed for the Task has get new insights concerning three main Italian aquifer systems extending in mountain areas. Given the strategic role of the mountain aquifers in terms of water supply, it is recommendable to continue, and possibly enhance, the monitoring activities, as well as to program specific surveys and modelling tools, for these kind of systems.

In these terms, the general approach adopted in the frame of Nextdata can represent a good reference for steering next actions.

REFERENCES

- Acocella, V. (2000): Space accommodation by roof lifting during pluton emplacement at Amiata (Italy). *Terra Nova*, 12, 149–155.
- Apollaro C., Accornero M., Marini L., Barca D., De Rosa R. (2009) The impact of dolomite and plagioclase weathering on the chemistry of shallow groundwaters circulating in a granodiorite-dominated catchment of the Sila Massif (Calabria, Southern Italy). *Appl. Geochem.*, 24, 957-979.
- Appelo C.A.J. and Postma D. (1996) *Geochemistry, groundwater and pollution*. A.A. Balkema, Rotterdam.
- Baldi, P., Bellani, S., Ceccarelli, A., Fiordelisi, A., Squarci, P. & Taffi, L. (1995): Geothermal anomalies and structural features of southern Tuscany. *World Geothermal Congress Proceedings Florence*, pp 1287–1291.
- Balestro G., Cadoppi P., Piccardo G.B., Polino R., Spagnolo G., Tallone S., Fioraso G., Lucchesi S., Forno M.G. (2009) Geological map of Italy at the scale 1:50:000, sheet 155 Torino Ovest. ISPRA, Istituto Superiore per la Protezione e la Ricerca ambientale, Roma.
- Baoxiang Z., Fanhai M. 2011. Delineation methods and application of groundwater source protection zone. *Water Resource and Environmental Protection (ISWREP)*, 2011 International Symposium on Volume: 1 (IEEE Conference Publications): pp 66–69
- Barazzuoli P., Bosco G., Nante N., Rappuoli D. e Salleolini M. (1994) The aquifer of Mount Amiata: Evaluation of the perennial yield and its quality. *Mem. Soc. Geol. It.*, 48, 825-832.
- Barazzuoli P., Capacci F., Gobbini M., Migliorini J., Rigati R. e Mocenni B. (2014) Valutazioni delle risorse idriche dell'acquifero contenuto nelle vulcaniti del Monte Amiata attraverso criteri strettamente idrologici. *Il Geologo*, Anno XXV, 94, 5-13.
- Batini, F., Bertini, G., Gianelli, G., Nicolich, R., Pandeli, E. & Puxeddu, M. (1986): Deep structure of the geothermal region of the Monte Amiata volcano (Tuscany, Italy). *Mem. Soc. Geol. It.*, 35, 755–759.
- Boccaletti, M., Elter, P. & Guazzone, G. (1971): Plate Tectonics models for the development of the western Alps and Northern Apennines. *Nature*, 234, 108-111.
- Bove A., Casaccio D., Destefanis E., De Luca D.A., Lasagna M., Masciocco L., Ossella L., Tonussi M. (2005) *Idrogeologia della pianura piemontese*. Regione Piemonte Direzione Pianificazione delle Risorse Idriche, Mariogros Industrie Grafiche S.p.A., Torino.
- Brogi, A. (2008): The structure of the Monte Amiata volcano-geothermal area (Northern Apennines, Italy): Neogene- Quaternary compression versus extension. *Int. J. Earth Sci.*, 97, 677–703.
- Brunet, C., Monie´ , P., Jolivet, L. & Cadet, J.P. (2000): Migration of compression and extension in the Tyrrhenian Sea: insights from 40Ar / 39Ar ages on micas along a transect from Corsica to Tuscany. *Tectonophysics*, 321, 127–155.

- Brussolo E., Ferraris S., Gisolo D., Doveri M., Masetti G., Provenzale A. (2008) Yearly water balance of the Piedmont Alpine zone. SISC 2018, Sixth Annual Conference – Recent trends in climate sciences, adaptation and mitigation.
- Canavese P.A., De Luca D.A., Masciocco L. (2004) La rete di monitoraggio delle acque sotterranee delle aree di pianura della Regione Piemonte: quadro idrogeologico. Prisma: il monitoraggio delle acque sotterranee nella Regione Piemonte, Regione Piemonte, 175pp.
- Capilongo L., Cotterchio C., Faliero P., Ferrero C., Latagliata V., Pantaleo B., Rinaldi A., Bortolami G., De Luca D.A., Masciocco L., Morelli A. (2003) Le acque sotterranee della pianura di Torino - Carta della base dell'acquifero superficiale - Note illustrative.
- Carmignani L., Kligfield R. 1990. Crustal extension in the Northern Apennines: the transition from compression to ex-tension in the Alpi Apuane Core Complex. *Tectonics*, v. 9, 6, 1275-1303.
- Carmignani, L., Decandia, F.A., Disperati, L., Fantozzi, P.L., Lazzarotto, A., Liotta, D. and Oggiano, G. (1995): Relationships between the Sardinia-Corsica-Provencal Domain and the Northern Apennines. *Terra Nova*, 7, 128–137.
- Celico P.B. (1987) Piano di Bacino del Fiume Fiora: studio idrogeologico preliminare. Relazione tecnica, VAMS Ingegneria s.r.l. - Ministero dei Lavori Pubblici Provveditorato alle OO.PP per la Toscana, pp. 50.
- Cerrina F. A., Da Prato S., Doveri M., Ellero A., Lelli M., Marini L., Masetti G., Nisi B. e Raco B. (2009). Caratterizzazione geologica, idrogeologica e idrogeochimica dei Corpi Idrici Sotterranei Significativi della Regione Toscana (CISS) 99MM020 “Acquifero dell’Amiata”. Report Regione Toscana, p. 44.
- Chiodini G., Frondini F., Marini L. (1995) Theoretical geothermometers and PCO₂ indicators for aqueous solutions coming from hydrothermal systems of medium-low temperature hosted into carbonate-evaporite rocks. Application to the thermal springs of the Etruscan Swell, Italy. *Appl. Geochem.*, 10, 337-346.
- Civita M., Forti P., Marini P., Meccheri M., Micheli L., Piccini L., Pranzini G. 1991. Carta della vulnerabilità all'inquinamento degli acquiferi delle Alpi Apuane “Pollution Vulnerability map for the aquifers of the Apuane Alps” – scala “scale” 1:25.000. Gruppo Nazionale per la Difesa dalle Catastrofi Idrogeologiche, C. N. R., SE.L.CA, Firenze.
- Conti P., Di Pisa A., Gattiglio M., Meccheri M. 1993. Prealpine basement in the Alpi Apuane (Northern Apennines, Italy). In: Von Raumer, J.F., Neubauer, F. (Eds.), *Pre-Mesozoic geology in the Alps*. Springer Verlag, 609-621.
- Cortecchi G., Lattanzi P., Tanelli G. 1985. Barite-iron oxide-pyrite deposits from Apuane Alps (Northern Tuscany, Italy). *Geol. Carpatica*, 36, 347-357.
- Craig H. 1961. Isotopic Variation in meteoric waters. *Science*, 133, 1702-1703.
- De Luca D. A., Osella L. (2014) Assetto idrogeologico della Città di Torino e del suo hinterland. *Geologia dell’Ambiente, Atti del simposio “Geologia urbana di Torino”, 1/2014: 10-15.*

- De Luca, D. A., Destefanis, E., Forno M. G., Lasagna, M., Masciocco, L., (2014) The genesis and the hydrogeological features of the Turin Po Plain fontanili, typical lowland springs in Northern Italy. *Bull Eng Geol Environ* 73:409–427. Lo Russo S., Taddia G. (2009) Groundwater in the Urban Environment: Management Needs and Planning Strategies. *Am. J. Environ. Sci.*, 5(4): 484-500
- Davis, J.C., 1986. *Statistics and Data Analysis in Geology*. John Wiley & Sons, Inc. Second Edition, New York, 646 pp.
- Doveri M. 2004. Studio idrogeologico e idrogeochimico dei sistemi acquiferi del bacino del Torrente Carrione e dell'antistante piana costiera. Tesi di Dottorato inedita, Università di Pisa, 178 pp.
- Doveri M. e Mussi M. (2014) Water Isotopes as Environmental Tracers for Conceptual Understanding of Groundwater Flow: An Application for Fractured Aquifer Systems in the "Scansano-Magliano in Toscana" Area (Southern Tuscany, Italy). *Water*, 6, 2255-2277.
- Doveri M., 2000. Studio idrogeochimico di sistemi acquiferi superficiali e profondi delle Alpi Apuane e della Valle del Serchio. Tesi di Laurea, Università di Pisa, a.a. 1999-2000, 245 pp.
- Doveri M., Grassi S., Menichini M. e Bellatalla M. (2013a) Dati e considerazioni a carattere idrodinamico sulle vulcaniti del Monte Amiata (Toscana meridionale). *Convegno IdroVulc2013, Riassunti*, 71-73.
- Doveri M., Menichini M. (2017) Aspetti idrogeologici delle vulcaniti nel Monte Amiata. In: *Il Vulcano di Monte Amiata*. a cura di Claudia Principe, Guido Lavorini e Luigina M. Vezzoli (eds.), pp. 255 - 265. ESA - Edizioni Scientifiche ed Artistiche, 2017 - Napoli, Italia.
- Doveri M., Menichini M., Cerrina Feroni A. 2013c. Stable water isotope as fundamental tool in karst aquifer studies: some results from isotopic applications in the Apuan Alps carbonatic complexes (NW Tuscany). *Italian Journal Engineering Geology and Environment* 1: 25-42.
- Doveri M., Menichini M., Provenzale A., Scozzari A. (2017) Effects of climate change on groundwater: observed and forecasted trends on Italian systems. *EGU General Assembly Conference Abstracts*, 19, 14440
- Doveri M., Menichini M., Provenzale A., Scozzari A. (2018a) Groundwater response to climate changes: examples of observed and modeled trends on Tuscany aquifers (central Italy). *Volume Atti Accademia Lincei giornata mondiale sull'acqua 2017*, in press.
- Doveri M., Menichini M., Scozzari A. 2016. Protection of groundwater resources: worldwide regulations, scientific approaches and case study. In: Scozzari A, Dotsika E (edited by): "Threats to the quality of groundwater resources: prevention and control" - *The handbook of environmental chemistry*, Springer-Verlag Berlin Heidelberg 2016, 40,13-30.
- Doveri M., Nisi B., Cerrina Feroni A., Ellero A., Menichini M., Lelli M., Masetti G., Da Prato S., Principe C., Raco B. (2012). Geological, hydrodynamic and geochemical features of the volcanic aquifer of Mt. Amiata (Tuscany, Central Italy): an overview. *Acta Vulcanologica*, Vol.24 (1-2), pp. 51-72.

- Doveri M., Nisi B., Ellero A., Menichini M., Lelli M., Masetti G., Da Prato S. e Raco B. (2013b) Geological-hydrogeological-geochemical integrated approach to characterize Significant Groundwater Bodies hosted in fractured rocks: the example of the Monte Amiata volcanic aquifer (Tuscany, Italy). *Epitome Geitalia* 2013, 269.
- Doveri, M., Piccini, L., Menichini, M. (2018b) Hydrodynamic and geochemical features of metamorphic carbonate aquifers and implications for water management: the Apuan Alps (NW Tuscany-Italy) case study. In: *Karst Water Environment: Advances in Research, Management and Policy* (T. Younos, M. Schreiber, K. K. Ficco, Editors). Springer Publishers (in press).
- Drysdale R. N., Pierotti L., Piccini L., Baldacci F. 2001. Suspended sediments in karst spring waters near Massa (Tuscany), Italy. *Environmental Geology* 40, 1037-1050.
- Fan Y. 2015. Groundwater. How much and how old? *News & Views, Nature Geoscience*, advance online publication, www.nature.com/naturegeoscience, 1-2.
- Ferrari, L., Conticelli, S., Burlamacchi, L. & Manetti, P. (1996): Volcanologic evolution of the Monte Amiata, Southern Tuscany: new geological and petrochemical data. *Acta Vulcanol.*, 8, 41-56.
- Fron dini F., Caliro S., Cardellini C., Chiodini G., Morgantini N. (2009) Carbon dioxide degassing and thermal energy release in the Monte Amiata volcanic-geothermal area (Italy). *Appl. Geochem.*, 24, 860-875.
- Gambardella B., Marini L. Baneschi I., (2005) Dissolved potassium in the shallow groundwaters circulating in the volcanic rocks of central-southern Italy. *Appl. Geochem.*, 20, 875-897.
- Garrels R. M. (1968) Genesis of some ground waters from igneous rocks In *Researches in Geochemistry* (ed. P. H. Abelson), Vol. 2, pp. 406-420. Wiley.
- Gat J.R., Carmi I. 1970. Evolution of isotopic composition of atmospheric waters in the Mediterranean sea area. *J. Geophys. Res.*, 75, 3032-3048.
- Gatt J.; Klein B.; Kushnir Y.; Roether W.; Wernli H.; Yam R.; Shemesh A. (2003). Isotope composition of air moisture over the Mediterranean Sea: an index of the air-sea interaction pattern. *Tellus B*, 55, 953 - 965.
- Harbaugh, A. W., Banta, E. R., Hill, M. C., McDonald, M. G., 2000. MODFLOW-2000, the U.S. Geological Survey modular ground-water model—User guide to modularization concepts and the Ground-water flow process. U.S. Geological Survey Open-File Report 00-92, 121 p.
- Hiscock K.M. 2011. Groundwater in the 21st century – meeting the challenges. In: Anthony J, Jones A (eds) *Sustaining groundwater resources: a critical element in the global water crisis*, in *International Year of Planet Earth*, pp 207-225.
- Irace, A., Clemente, P., Natalicchio, M., Ossella, L., Trenkwalder, S., De Luca, D. A., Mosca, P., Piana, F., Polino, R. & Violanti, D. (2009). *Geologia e idrostratigrafia profonda della Pianura Padana occidentale*. Edizioni La Nuova Lito, Firenze, 1-135.

- Irace, A. Clemente, P., Piana, F., De Luca, D.A., Polino, R., Violanti, D., Mosca, P., Trenkwald, S., Natalicchio, M., Ossella, L., Governa, M. & Petricig, M. (2010). Hydrostratigraphy of the late Messinian-Quaternary basins in the southern Piedmont (northwestern Italy). *Mem. descr. Carta Geol. It.*, 90, 133-152, ISSN: 0536-0242.
- Jolivet, L., Daniel, J.M., Truffert, C. & Goffe', B. (1994). Exhumation of deep crustal metamorphic rocks and crustal extension in back-arc regions. *Lithos*, 33, 3-30.
- Lelli, M. 2017. Caratterizzazione chimica delle acque circolanti all'interno del Complesso Vulcanico del Monte Amiata. In "Il vulcano di Monte Amiata", Eds. C. Principe, G. Lavorini, L. Vezzoli, pp. 267-280.
- Lucchesi (2001) Sintesi preliminare dei dati di sottosuolo della pianura piemontese centrale. *Ge.am*, 103, 115-121
- Mancini S., 2004. La buca dell'Angina grotta e miniera apuana. www.alpiapuane.info.
- Mantelli F., Lotti L., Montigiani A., Piccini L. 2015. Chimica delle acque del Complesso carsico del Monte Corchia. *Acta Apuana*, XI (2012), 33-45.
- Mantelli F., Piccini L. 2007. Caratteristiche chimiche delle acque delle sorgenti carsiche delle Alpi Apuane. In: Comitato Alpi Apuane 2007, "Apuane e dintorni - Guida incompleta al fenomeno carsico", Tip. Amaducci, Borgo a Mozzano, Lucca, 69-75.
- Marroni M., Moratti G., Costantini A., Conticelli S., Benvenuti M. G., Pandolfi L., Bonini M., Cornamusini G. e Laurenzi M. A. (2015) Geology of the Monte Amiata region, Southern Tuscany, Central Italy. *Ital. J. Geosci.*, 134, 171-199.
- Martinetto E., Scardia G., Varrone D. (2007) Magnetobiostratigraphy of the Stura di Lanzo fossil forest succession. *Riv. Ital. Paleontol. Stratigr.* 113 (1), 109-125.
- Martinez Navarrete C., Grima Olmedo J, Duran Valsero J.J., Gomez J.D., Luque Espinar J.A., de la Orden G.J.A., 2008. Groundwater protection in Mediterranean countries after the European water framework directive. *Environ Geol* 54:537-549.
- Menichini M., 2012. A multidisciplinary approach to define the hydrogeological model of aquifer systems in the "Fiume Versilia" catchment and the adjacent coastal plain (Northwest Tuscany, Italy). Tesi di Dottorato inedita, Università di Pisa, Scuola di Dottorato Galileo Galilei. Programma in Scienze della Terra.
- Menichini M., Doveri M., El Mansoury B., El Mezouary L., Lelli M., Raco B., Scozzari A., Soldovieri F., 2016. Groundwater vulnerability to climate variability: modelling experience and field observations in the lower Magra Valley (Liguria, Italy). *Geophysical Research Abstracts*, Vol. 18, EGU2016-15483.
- Menichini M., Doveri M., Piccini L. 2016. Hydrogeological and geochemical overview of the karst aquifers in the Apuan Alps (Northwestern Tuscany, Italy). *Italian Journal of Groundwater*, AS16-198: 15-23.
- Minissale A., Magro G., Vaselli O., Verrucchi C., Perticone I. (1997). Geochemistry of water and gas discharges from the Mt. Amiata silicic complex and surrounding areas (central Italy). *Journal of Volcanology and Geothermal Research*, 79, 223 -251.

- Molli G., Cortecci G., Vaselli L., Ottria G., Cortopassi A., Dinelli E., Mussi M., Barbieri M. 2010. Fault zone structure and fluid-rock interaction of a high angle normal fault in Carrara marble (NW Tuscany, Italy). *Journal of Structural Geology* 32, 1334-1348.
- Molli G., Doveri M., Manzella A., Bonini L., Botti F., Menichini M., Montanari D., Trumpy E., Ungari A., Vaselli L. 2015. Surface - subsurface structural architecture and groundwater flow of the Equi Terme hydrothermal area, northern Tuscany Italy, *Italian Journal of Geosciences*, vol. 134, 442-457.
- Molli G., Meccheri M. 2012. Structural inheritance and style of reactivation at mid-crustal levels: A case study from the Alpi Apuane (Tuscany, Italy). *Tectonophysics* 579, 74-87.
- Molli, G. (2008): Northern Apennine–Corsica orogenic system: an updated review. *Geol. Soc. London Spec. Publ.*, 298, 413– 442.
- Mussi M., Leone G., Nardi I. 1998. Isotopic geochemistry of natural water from the Alpi Apuane-Garfagnana area, Northern Tuscany, Italy. *Miner. Petrogr. Acta* 41, 163-178.
- Orsini A. 1987. Indagine idrogeologica e geochimica ai fini della ricostruzione dei bacini di alimentazione di alcuni sorgenti nella zona delle Apuane. Tesi di laurea in Scienze Geologiche, Facoltà di Scienze M.F.N., Università degli Studi di Firenze, 124 pp.
- Ottria, G., Molli G. 2000. Superimposed brittle structures in the late-orogenic extension of the Northern Apennine: results from the Carrara area (Alpi Apuane, NW Tuscany). *Terra Nova* 12: 52-59.
- Piana, F., Fioraso, G., Irace, A., Mosca, P., d'Atri, A., Barale, L., Falletti, P., Monegato, G., Morelli, M., Tallone, S., Vigna, G.B., 2017. Geology of Piemonte region (NW Italy, Alps-Apennines interference zone). *J. Maps* 13 (2), 395–405.
- Piccini L. 2002. Acquiferi carbonatici e sorgenti carsiche delle Alpi Apuane “Carbonate aquifers and karst springs of Apuan Alps”. *Atti Conv. “Le risorse idriche sotterranee delle Alpi Apuane: conoscenze attuali e prospettive di utilizzo”*, Forno di Massa, Giugno 2002: 41-76.
- Piccini L., Giannini E., Malcapi V., Poggetti E., Steinberg B. 2015. Monitoraggio idrodinamico di un sistema carsico: risultati preliminari di un anno d’indagini alla sorgente Pollaccia (Alpi Apuane – Toscana). *Atti Convegno “La ricerca carsologica in Italia”*, Fabrosa Soprana (CN), 22-23 giugno 2013, 147-154.
- Piccini L., Pranzini G., Tedici L., Forti P. 1999. Le risorse idriche dei complessi carbonatici del comprensorio apuo-versiliense “water resources of carbonate complexes in apuan-versilian region”. *Quaderni Geologia Applicata* 6-1, 61-78.
- Principe C., Vezzoli L., La Felice S. (2017) Stratigrafia ed evoluzione geologica del vulcano di Monte Amiata. In: *Il Vulcano di Monte Amiata*. a cura di Claudia Principe, Guido Lavorini e Luigina M. Vezzoli (eds.), pp. 85 - 101. ESA - Edizioni Scientifiche ed Artistiche, 2017 - Napoli, Italia.
- Regione Piemonte, Direzione Pianificazione Risorse Idriche (2005) *Idrogeologia della pianura Piemontese “Hydrogeology of the piedmont plain”*, Mario Gros Industrie Grafiche SpA Torino 15 pp..

- Regione Piemonte, Direzione Pianificazione Risorse Idriche (2007) Piano di Tutela delle acque, rev 03. "Water protection plan", 23 pp.
- Regione Piemonte, Direzione Ambiente, Governo e Tutela del Territorio (2018) Progetto di revisione, Piano di Tutela delle acque "Revision Project, Water protection Plan", 282 pp.
- Rosegrant M.W., Cai X., Cline S.A. 2002. World Water and Food to 2025: dealing with scarcity. International Food Policy Research Institute, Washington, 322 pp.
- Siebert S, Burke J, Faures J M, Frenken K, Hoogeveen J, Döll P, Portmann F T (2010) Groundwater use for irrigation – a global inventory. *Hydrol Earth Syst Sci*, 14: 1863-1880.
- Singh, A., Singh, A. K., & Engelhardt, M. (1997). The Lognormal Distribution in Environmental Applications. Technology Support Center Issue, EPA/600/S-97/006.
- Strandberg, G., L. Bärring, U. Hansson, C. Jansson, C. ones, E. Kjellström, M. Kolax, M. Kupiainen, G. Nikulin, P. Samuelsson, A. Ullerstig and S. Wang. (2014). CORDEX scenarios for Europe from the Rossby Centre regional climate model RCA4. SMHI, Report Meteorology and climatology No. 116. Available at: <http://urn.kb.se/resolve?urn=urn:nbn:se:smhi:diva-2839>.
- Tassi F., O. Vaselli, F. Cuccoli, A. Bucciati, B. Nisi, E. Lognoli and G. Montegrossi. 2009. A geochemical multi-methodological approach in hazard assessment of CO₂-rich gas emissions at Mt. Amiata volcano (Tuscany, central Italy). *Water Air Soil Poll. Focus*, 9, 117-127. DOI10.1007/s11267-008-9198-2.
- Taylor R., Scanlon B., Doll P., Rodell M. et al. 2013. Ground water and climate change. *Nature climate change*, 3:322-329
- Vaselli L., Cortecci G., Tonarini S., Ottria G., Mussi, M. 2012. Conditions for veining and origin of mineralizing fluids in the Alpi Apuane (NW Tuscany, Italy): Evidence from structural and geochemical analyses on calcite veins hosted in Carrara marbles. *Journal of Structural Geology* 44, 76-92.
- Vaselli, O., Rappuoli, D., Nisi, B., Bianchi, F., Tassi, F., Cabassi, J., Giannini, L., Magi, F., Capecchiacci, F., Maddii, V., 2017. Geochimica delle acque di Galleria Italia (Abbadia San Salvatore, Siena). In "Il vulcano di Monte Amiata", Eds. C. Principe, G. Lavorini, L. Vezzoli, pp. 283-302.
- VV. AA. 2010. "Indagine geochimica ed isotopica delle acque termo- ed oligo-minerali dell'area amiatina. MAC-GEO Project, Regione Toscana, 45 pp.
- WBCSD (2006) Facts and trends – water. World Business Council for Sustainable Development. <http://www.wbcsd.org/Pages/EDocument/EDocumentDetails.aspx?ID=137>. Accessed 10 Sept 2014.
- Wolery T.W., Jarek R.L. (2003) Software user's manual. EQ3/6, Version 8.0. Sandia National Laboratories – U.S. Dept. of Energy Report.
- Zhu Y. Balke K. D. 2008. Groundwater protection: what can we learn from Germany? *J. Zhejiang Univ Sci B* 9(3):227–231.